SECURITY CLASSIFICATION OF THIS PAGE (When Data Entered)

REPORT DOCUMENTATION PAGE		READ INSTRUCTIONS BEFORE COMPLETING FORM
1. REPORT NUMBER NRL Report 7925	2. GOVT ACCESSION NO.	3. RECIPIENT'S CATALOG NUMBER
4. TITLE (and Subtitle) INVESTIGATION OF THE STIMULATION OF ULF WAVES		5. TYPE OF REPORT & PERIOD COVERED Interim report on one phase of the NRL problem 6. PERFORMING ORG. REPORT NUMBER
7. AUTHOR(s) John W. Willis and John R. Davis		8. CONTRACT OR GRANT NUMBER(s)
9. PERFORMING ORGANIZATION NAME AND ADDRESS Naval Research Laboratory Washington, D.C. 20375		10. PROGRAM ELEMENT, PROJECT, TASK AREA & WORK UNIT NUMBERS NRL Problem R07-23 Project RF21-222-402
11. CONTROLLING OFFICE NAME AND ADDRESS Department of the Navy Office of Naval Research Arlington, Virginia 22217		12. REPORT DATE November 13, 1975 13. NUMBER OF PAGES 38
14. MONITORING AGENCY NAME & ADDRESS(if different from Controlling Office)		15. SECURITY CLASS. (of this report) Unclassified 15a. DECLASSIFICATION/DOWNGRADING SCHEDULE

16. DISTRIBUTION STATEMENT (of this Report)

Approved for public release; distribution unlimited.

17. DISTRIBUTION STATEMENT (of the abstract entered in Block 20, if different from Report)

18. SUPPLEMENTARY NOTES

19. KEY WORDS (Continue on reverse side if necessary and identify by block number)

Ultra-low frequencies (ULF)	Ionospheric heating
Communications to submerged vehicles	VLF wave interaction
Magnetosphere	Micropulsations
Magnetospheric ion injection	Geomagnetic variations
Plasma cloud	Magnetic-field sensors

20. ABSTRACT (Continue on reverse side if necessary and identify by block number)

Two methods of artificially stimulating ultra-low-frequency (ULF) waves in the ionosphere have been investigated experimentally. Radio-frequency heating of the ionospheric-dynamo-current region has been attempted using a high-frequency transmitter and has been found to be ineffective.

Pulse modulation of the U.S. Navy VLF transmitter at Cutler, Maine, has been explored as a means of stimulating geomagnetic micropulsations. In a month-long experiment the transmitter

(continued)

DD FORM 1 JAN 73 1473 EDITION OF 1 NOV 65 IS OBSOLETE
S/N 0102-014-6601

SECURITY CLASSIFICATION OF THIS PAGE (When Data Entered)

(20 continued)

was square-wave modulated at frequencies of 0.2, 1, and 5 Hz, with a network of sensitive magnetometers employed as micropulsation detectors. Though the experimental results are not statistically conclusive, micropulsations occurred on several occasions at harmonics of the transmitter modulation frequency. It is likely that ULF waves may be stimulated by this means under magnetically quiet conditions immediately following geomagnetically active days.

It is concluded that practical means of emitting ULF waves for global communications are prohibitively expensive by comparison to other alternatives in the extremely-low-frequency or higher bands.

CONTENTS

PREFACE iv

INTRODUCTION 1

STIMULATION METHODS 4

RF Heating 4
VLF-ULF Wave-Wave Interaction 6

VLF-ULF EXPERIMENT 7

RESULTS 10

DISCUSSION 15

CONCLUSION 17

ACKNOWLEDGMENTS 18

APPENDIX A – Radio-Frequency Heating Effects in the Lower E Region 19

APPENDIX B – Data Catalog 28

REFERENCES 32

PREFACE

The problem of artificial stimulation of ultra-low frequency (ULF) waves as a potential means of communications to underwater terminals has been discussed in detail in a previous report [1]. A number of unusual methods were suggested as generating mechanisms for ULF waves. It is the purpose of this report to discuss the implementation of these methods and in particular the results of an experiment using very-low-frequency (VLF) waves as a ULF stimulation source. For the convenience of the reader the salient points of the previous discussion of ULF generation will be briefly presented in what follows. For a more complete background to the problem, the reader is referred to the earlier report.

INVESTIGATION OF THE STIMULATION OF ULF WAVES

INTRODUCTION

In recent years the increasing importance of underwater-based tactical systems has provoked new inquiries into the problems of long-range, mixed-medium communications. Conventional electromagnetic methods undergo sizable losses in seawater, and, conversely, acoustic techniques which have been employed underwater have limited range in air. The trend has been to seek operable one-way electromagnetic communications at lower frequencies from high-power, fixed-site transmitters of which the Navy VLF transmitters (15 - 30 kHz) are examples and a proposed extremely-low-frequency (ELF) communication system (10 - 100 Hz) represents the state of the art. Because of the difficulty of radiating extremely-long-wavelength electromagnetic waves, the ELF transmitting antenna [2] must have large physical size (tens of elements tens of kilometers in length). This cumbersome size is offset by the predicted large geographical coverage and improved underwater penetration of ELF waves relative to VLF waves. A logical extension of this approach is to investigate the potential of ULF (frequencies less than 10 Hz) as a means of communicating with underwater stations.

The principal advantages of proceeding to yet lower frequencies than ELF are the following:

- Low attenuation in seawater: the skin depth for a 0.5-Hz wave in ordinary seawater is over 300 m.
- Large illuminated area: naturally occurring ULF waves propagate as magnetohydrodynamic waves over extended distances along the field lines in the magnetosphere and, it is now believed, in an ionospheric waveguide centered on the F-layer density peak [3].
- Magnetospheric amplification: resonant wave-particle interactions with high-energy protons in the magnetosphere could provide as much as 30-dB of amplification [4, 5].
- Low attenuation in the ionospheric waveguide: attenuation at night in the ionospheric duct is calculated at 1 - 2 dB/1000 km. In the daytime ionosphere the rate is some two to three times higher [6].
- Possibility of channeling in specific directions: theory suggests that the ducted waves may be channeled in N-S or E-W directions [7].

Against these factors must be weighed the following disadvantages:

- Low information rate: messages would necessarily be simple and concise.
- Difficulty in generation: conventional antennas require enormous dimensions and power to obtain fields of significant amplitudes in the ionospheric waveguide at ULF frequencies.
- Motion-sensitive antennas: the normal receiving antennas at these low frequencies are inductive and hence sensitive to induced signals due to antenna motion in the earth's magnetic field.

Such information as we do have regarding ULF propagation has been garnered from observations of natural signals in the frequency range of 0.2 - 5 Hz. These signals are detected on the earth's surface as micropulsations of the earth's magnetic field. By international convention the narrow-band micropulsations which occur as repetitive pulse trains between 0.2 and 5 Hz are known as Pc 1, and it is their properties which are of particular interest for communications. Briefly the observed characteristics of Pc 1 micropulsations are [3, 8]:

- They occur alternately at magnetically conjugate stations, with a phase relationship indicating that the waves propagate back and forth along the geomagnetic field lines joining the stations.
- They are often observed to commence at low amplitudes, and increase in size over a time interval of tens of minutes.
- They appear as an extended pulse train of relatively narrow-bandwidth wave packets tens of seconds in length separated by intervals of several seconds.
- They generally have a spectral variation which suggests dispersive propagation in the magnetosphere.
- They are detected most strongly in the auroral regions.
- They appear to propagate to lower latitudes with group velocities on the order of several hundred km/s in an ionospheric-waveguide duct.
- They are attenuated in the duct by about 1 - 2 dB/1000 km at night and at several times that rate during the daytime.

Present understanding of natural ULF waves is illustrated in Fig. 1.* Figure 1 is a sketch of the earth, ionosphere, and magnetosphere in which the prominent features of this process are indicated. The closed circle at the left represents the earth, and the stippled ring encircling it illustrates the ionospheric duct described previously. The boundaries of the duct are nominally 100 and 2000 km above the surface of the earth. The wedge-shaped, cross-hatched region is a rough indication of that region of the magnetosphere in which protons, of the proper energy spectrum to interact with ULF waves and amplify them, are trapped. The eccentric circles passing between the northern and southern hemispheres of the earth are a schematic representation of the magnetic field on the earth. The labels $L = 2$ to $L = 9$, which appear in the equatorial plane, represent parameters of a geomagnetic coordinate system and indicate the distance in earth radii of each geomagnetic field line from the center of the earth in the equatorial plane. The trapped-proton region extends from about $L = 2.6$ to $L = 6$.

Without specifying, for the meantime, the means by which a ULF wave is generated, let us suppose that such a wave is launched in an appropriate Magnetohydrodynamic (MHD) mode from the ionosphere in the northern auroral zone. The mode of interest is a left-hand-polarized, slow Alfven wave, because this particular type of MHD wave will be guided by the magnetic field and channeled into the proton belt. In Fig. 1 this channeling is indicated as taking place

*A discussion similar to the following appears in Ref. 1 but is repeated here for the reader's convenience.

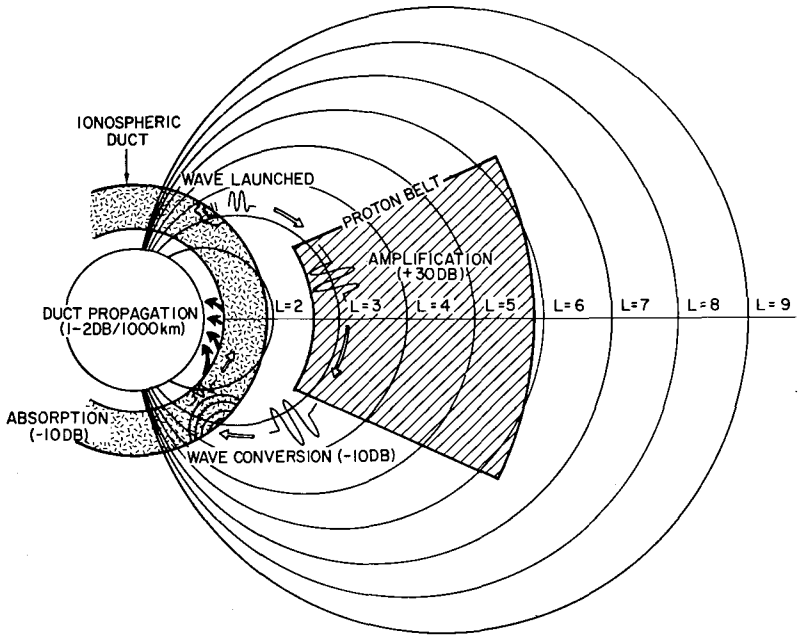

Fig. 1 – Earth, ionosphere, and magnetosphere with magnetospheric proton-belt amplification

along the L = 3 contour. On entering the proton belt, the ULF wave will interact with the resident protons by a mechanism which is reminiscent of a traveling-wave-tube amplifier. That is, for a wave whose sense of polarization is the same as the direction in which the protons are spiraling around the direction of the magnetic field and whose frequency (when doppler shifted) equals the frequency of particle rotation, a transfer of energy can take place from the gyrating particles to the wave. This process is analogous to a traveling-wave tube in which the spiraling-proton beam forms a slow-wave structure. As indicated in Fig. 1, an amplification limit of about 30 dB is probable [4, 5]. This value is consistent with the results of observations of natural micropulsations and indicates that there is not an inexhaustible supply of protons with the proper energy and spiral pitch angle for coupling with the ULF wave.

On emerging from the proton belt, the amplified ULF wave continues to be guided by the magnetic field and impinges on the ionosphere. Figure 1 shows this event taking place in the southern hemisphere.

The left-hand-polarized wave is partially absorbed in the lower ionosphere. It can be detected in a small region on the earth directly below its point of impingement on the ionosphere, due to the quasi-evanescent wave fields which penetrate to and below the surface of the earth. However, a process which occurs within the ionospheric E region above the altitude of high absorption for these waves permits further low-loss propagation to proceed away from the ionospheric source region. In the ionospheric E region, a mode-conversion process takes place in which the left-hand-polarized, slow Alfven wave is converted to a (locally-right-hand-polarized) fast Alfven wave. The latter mode suffers considerable absorption when passing downward through the lower ionosphere but, more importantly, is ducted horizontally by the ionosphere above this absorbing region. As is indicated in Fig. 1, the wave-conversion process entails a loss of about 10 dB. This value is consistent with observations of natural phenomena and accounts for energy which is coupled into other modes as well as energy which is reflected back along the direction of the

magnetic field toward the proton belt (where, incidentally, it can be further amplified and in the the case of Pc 1 micropulsations gives rise to subsequent pulses in the long train of wave packets which is typically observed). We also have indicated in Fig. 1 an absorption of about 10 dB in the lower ionosphere. This figure, which also is motivated by observations of natural phenomena [6], accounts for collision-related losses in the ionospheric D region. It may be an overestimate for the darkened hemisphere, where some measurements suggest that there is very little absorption in the nighttime D region.

Finally, there occurs the process of ducted propagation which, as indicated in Fig. 1, takes place with an attenuation rate as low as 1 dB/1000 km [6]. It is likely that so low an attenuation rate will hold only for an undisturbed ionosphere in darkness. In the sunlit hemisphere, an attenuation rate of 3 - 5 dB/1000 km is probably more realistic [8]. We have sketched a series of solid arrows at the bottom of the duct, indicating that energy leaks from the lower boundary of the duct to points on and beneath the surface of the earth. This energy reaches the earth by means of the quasi-evanescent wave fields which extend below the duct boundary. Once again, observations of natural phenomena, supplemented by a considerable theoretical effort, have served as the basis for these estimates of attenuation rate.

In Fig. 2 a representative Pc 1 micropulsation is illustrated in both amplitude and spectral displays. This micropulsation event was detected at five sites in the Eastern United States, as shown, and the substantial integrity of its detailed structure was preserved at all sites.

STIMULATION METHODS

To date the only man-made ULF signals have been obtained in connection with nuclear detonations in the upper atmosphere [9]. It has been proposed [10, 11] that a giant current loop 200 km across could function as a vertical magnetic dipole. Carrying 1000 A, it is calculated that a sufficiently large wave could be coupled into the ionospheric waveguide to bring about a 10-mγ (1 $\gamma = 10^{-5}$ gauss) signal at a distance of 5000 km. Alternatively, Greifinger and Griefinger [7] suggested similar results would be obtained from a 30-km-long, 500-A electric dipole antenna. The large cost involved and the considerable uncertainties that remain regarding ULF propagation make it unlikely that such a device could be constructed in the foreseeable future.

In an attempt to take a less conventional approach to the generation problem, we have proposed [1] several mechanisms for generating ULF waves which would take advantage of their natural characteristics. Among these other methods were lithium injection in the magnetosphere and cesium releases in the lower ionosphere. The two most viable mechanisms examined were modulation of the ionospheric dynamo currents via radio-frequency (RF) heating and magnetospheric wave-wave interaction using high-power VLF transmitters as a source.

RF Heating

The advent of high-powered (1 MW or greater) RF transmitters [12] designed specifically to perturb the ambient parameters of the ionosphere introduced a new dimension to active experimentation in the ionosphere. The ability to create controlled, repeatable effects at ionospheric heights is unique to these devices (specifically, in the United States, the transmitters at Arecibo, Puerto Rico, and Platteville, Colorado). The basic notion behind using an RF heater as a generator for ULF waves is that the ionospheric dynamo current is so large that a 0.05%

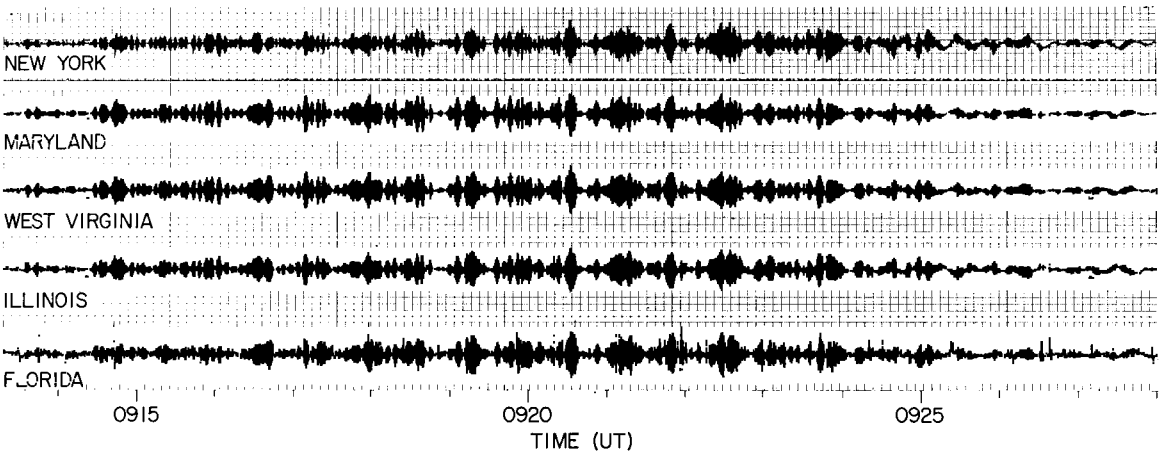

Fig. 2a – Waveforms of a typical Pc 1 event observed 15 April 1975 at NRL's five-site micropulsation network in the eastern United States. Data for sites at Canandaigua, New York, Stump Neck, Maryland, Huntington, West Virginia, Urbana, Illinois, and Panama City, Florida are shown from top to bottom.

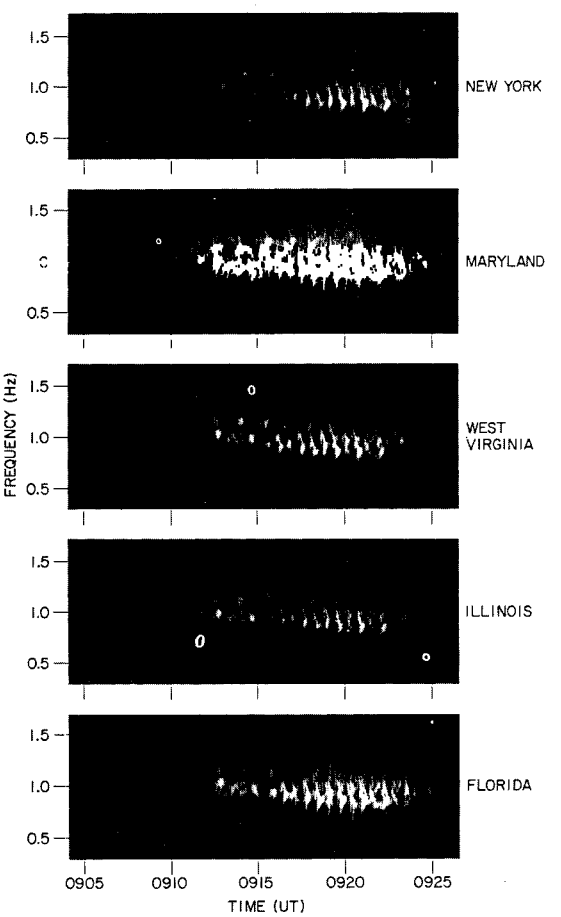

Fig. 2b – Spectral display of the data in Fig. 2a

variation in this current, if brought about rapidly (for example, with a time scale of about 1 s) should be easily visible as a fluctuation in the induced magnetic field on the earth.

An RF heater operating in the 2.5 - 10-MHz range and directed vertically increases the average energy of the electrons as the wave passes through the lower ionosphere. This effect is a result of the small mass of the electrons relative to the neutrals with which they collide. Though the energy taken out of the wave in this manner is generally fairly small, the resultant rapid (milliseconds) temperature increase for the electrons can be relatively large (tens or even hundreds of degrees with currently available transmitter power). In the lower ionosphere (90 - 140 km) this electron-temperature increase is followed by a slower (tens of seconds) increase in electron density due to the inverse temperature dependence of the dissociative recombination coefficient [13]. This density variation, which follows the transmitter signal and which would be expected to occur over an area of hundreds of square kilometers, should be sufficient to perturb the ionospheric dynamo current through the direct dependence of the ionospheric conductivity on the electron density.

We have presented elsewhere [14] an initial calculation of the density and temperature perturbations to be anticipated above the Platteville transmitter in the lower ionosphere. Since the appearance of our earlier work, the low-frequency capability of that facility has been extended down to 2.7 MHz, thus introducing the possibility of resonant absorption in the E layer. To account for this change, the calculation was extended in Appendix A to include lower frequencies and to further refine the approach taken previously by explicitly including the temperature dependence of the collision frequency $\nu(T)$. These changes affected both the power absorbed at the heights of interest as well as the losses incurred in the D region. The latter are of interest because experiments have demonstrated substantial crossmodulation effects in the D region as a result of perturbations of the collision frequency by the Platteville transmitter [15].

The results of these calculations stimulated a three-week-long experiment in the Fall of 1972 in which the Platteville RF transmitter was square-wave modulated at frequencies in the ULF band. Two three-axis magnetometer sites were established, one at a 10-km distance from the transmitter at Greeley, Colorado, and another 100 km away at Cheyenne, Wyoming. The Greeley station was overwhelmed by a near-field signal from the transmitter, and even the telephone lines in that vicinity were sensitive to the one-second-on, one-second-off modulation. At Cheyenne no positive identification of a transmitter signal at several frequencies and with several modulation schemes could be made, even with 30 minutes of coherent integration. We do not present further detail regarding this experiment and report its conduct here only for completeness. It is our conclusion that any effects that could have been stimulated by the Platteville transmitter were below geomagnetic noise and consequently that reasonable RF power levels are incapable of producing a useful signal under normal midlatitude ionospheric conditions.

VLF-ULF Wave-Wave Interaction

In an experimental study, Fraser-Smith [16] found indications that ULF whistler events were correlated in time with atmospheric discharges. He proposed that the low-frequency tail of the discharges has sufficient power in the ULF band to propagate into the magnetosphere and trigger a series of hydromagnetic emissions. Since such powerful atmospheric discharges are known to be the source of large-amplitude VLF whistlers, a reasonable alternative hypothesis would involve large amplitude, discharge-produced VLF whistlers in a nonlinear interaction in the magnetosphere to produce ULF whistlers. In this case a VLF whistler would act as an

indirect link between an atmospheric discharge and a hydromagnetic whistler. As further evidence for a naturally occurring ULF-VLF interaction, other experimenters [17, 18] have noted that VLF emissions are often amplitude modulated at periods in the 1 - 60-s range.

Recently this interaction has been considered in calculations by Harker et al. [19]. They considered an interaction represented by the synchronism parallelogram in Fig. 3, in which two VLF whistlers traveling almost parallel to the magnetic field line mix to yield a product ULF wave at the difference frequency traveling in the same direction. The two axes are dimensionless representations of the wave frequency and propagation vector, with Ω_{ce} and Ω_{ci} the normalized electron and ion gyrofrequencies respectively. When the actual ratio Ω_{ce}/Ω_{ci} for protons is included in the synchronism relations, the VLF interaction frequency is found to be at 0.95 Ω_{ce}. For the typical set of parameters chosen, the calculation of Harker et al. [19] estimated that ULF waves of about 1 mγ might be generated in the magnetosphere.

VLF-ULF EXPERIMENT

Prompted by the tentative link between VLF sources and ULF waves, an experiment was designed using the high-powered U.S. Navy transmitter (NAA) at Cutler, Maine, as a source for a nonlinear ULF-VLF interaction. To prescribe the experimental conditions for creating the large-amplitude VLF fields in the magnetosphere required to trigger an interaction, it is useful to consider the frequency range in which VLF magnetospheric amplification is observed naturally and to investigate the sites of available transmitters for appropriate paths. Natural VLF whistlers are commonly observed at between 0.3 and 0.5 of the equatorial electron gyrofrequency on the field line which passes through the ionospheric entry point of the whistler. For Pc 1 micropulsations the observed frequency range is between 0.3 and 0.7 of the equatorial proton gyrofrequency along a similarly defined magnetic field line.

These natural-amplification regions have been sketched in Fig. 4 as a graph of frequency versus geomagnetic latitude. The solid lines refer to the left-hand scale and indicate the limits on VLF whistlers. The dotted lines describe the ULF whistlers and are referred to the right-hand scale. Superimposed on this picture are the normal operating frequencies and tuning ranges for three powerful U.S. Navy transmitters and for the lower powered but strategically placed experimental instrument operated by Stanford University. From this figure it appears that NAA (Cutler,

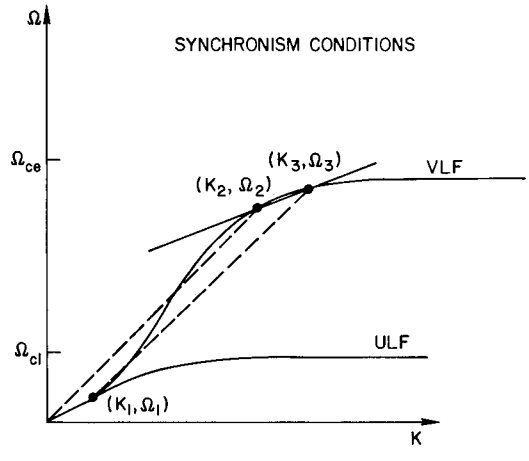

Fig. 3 – Wave-matching conditions (dashed lines) for a three-wave interaction using the ULF and VLF dispersion relations plotted against dimensionless wave vector and frequency (from Harker et al. [19]).

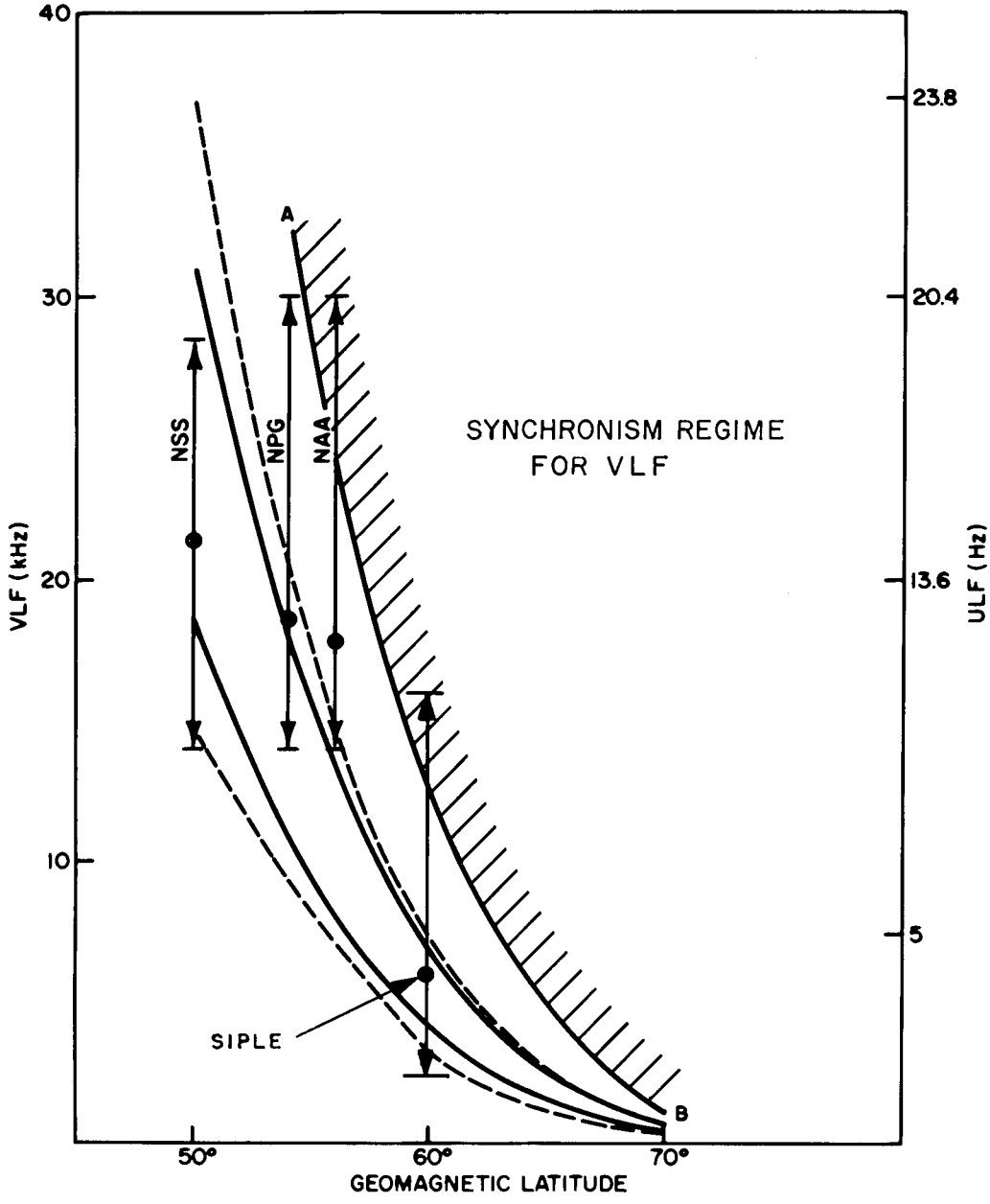

Fig. 4 – VLF transmitter frequencies (solid lines and left-hand scale) and ULF modulation frequencies (dashed lines and right-hand scale) appropriate for the magnetospheric three-wave interaction experiment. Tuning bands and operating frequencies are shown for three U.S. Navy transmitters between 50° and 60° North Geomagnetic Latitude. At a given latitude an appropriate VLF carrier frequency falls between the two solid lines, and an appropriate ULF modulation frequency falls between the two dashed lines.

Maine) is best situated (L = 3.5), of the high-powered transmitters (1.3 MW radiated at 14.7 kHz), to take advantage of VLF amplification on a field line also suited to ULF amplification at a reasonably low frequency. For instance, simultaneous magnetospheric amplification might be possible for an NAA launched VLF signal at 15 kHz and a ULF resultant at 5 Hz. Also shown (cross-hatched) is the higher frequency synchronism region that results from the considerations of Harker et al. [19].

In October 1973, NAA was modified to operate in a double-sideband, suppressed-carrier mode at 14.7 kHz, with separation frequencies chosen in the ULF band at 2, 4, and 8 Hz. It was thought that this two-frequency mode would optimize the possibility of a nonlinear interaction with a resultant at the separation frequency. Three-axis, ferrite-core magnetometers were deployed (Fig. 5) at Rangely, Maine, (265 km west of the transmitter) and Bermuda (1400 km from the transmitter on a magnetic north-south line). In addition a triangular grid of two-axis sensors was maintained in continuous operation at Canandaigua, N.Y., Indian Head, Md., and Huntington, W.Va.* These instruments have been proven sensitive to signals of less than 0.5 mγ at 1 Hz. The transmitter was operated in the two-frequency mode for alternate half-hours, eight hours a night. Because of a variety of technical problems, the experiment was reduced to 11 successful runs of this type during the period 7 - 27 October 1973. During this period there occurred only one ULF micropulsation event, and that showed no relation whatsoever to the transmitter operation. However, only three of these runs were at a low sidetone separation

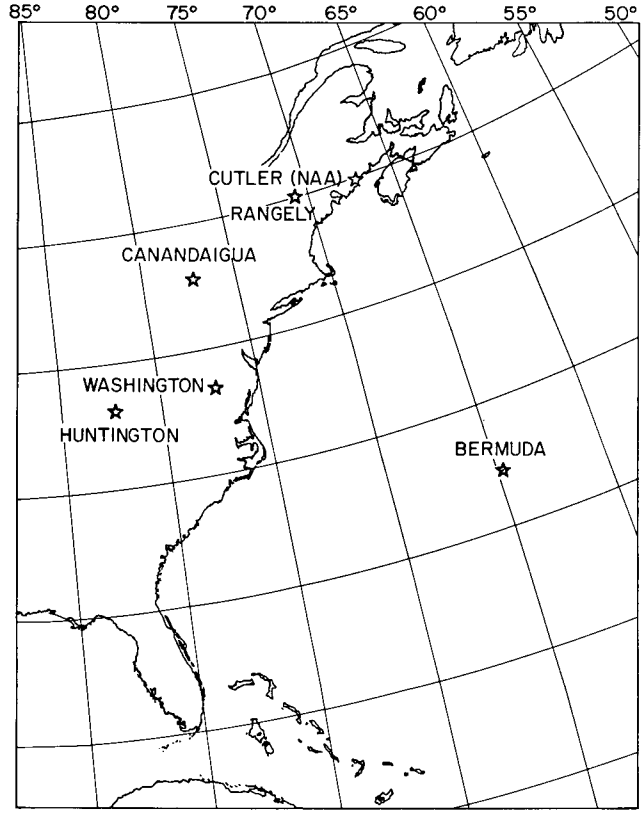

Fig. 5 — Field sites for VLF-ULF experiments (geographic coordinates)

*This network has been expanded since the experiment described here to the five sites whose data are described in Fig. 2.

frequency, 2 Hz, where Pc 1 events are more common at this latitude. Thus, in that it did not explore a large range of magnetospheric conditions, this experiment was not conclusive, but neither was it very encouraging.

At the same time preliminary results [20] from pulsemodulating the lower power transmitter at Siple in the Anarctic (4-kW radiated power, L = 4.1) showed a strong indication of a link between the start of a Pc 1 event and the operation of the transmitter. All of the 21 Pc 1 events which occurred were traced back to the 20 minutes of each half hour during which the transmitter operated in the pulsed mode.

To investigate the question of VLF-ULF interaction more thoroughly, we decided to again attempt to use the Cutler transmitter as a stimulus, this time using pulse modulation of the VLF transmitter at ULF rates. During October 1974, a three-axis-magnetometer field site was located at Winter Harbor, Maine (65 km from the transmitter), in addition to the triangular grid mentioned previously. The Cutler transmitter was operated at the same power level as before, but this time the 14.7-kHz carrier was on-off keyed at 0.2-, 1-, and 5-Hz rates with a 50% duty cycle. This mode was scheduled for alternate half-hours, twelve hours nightly, from 1 - 28 October 1974, with different modulation frequencies on successive nights. There were numerous late starts and occasional power outages which interfered with this schedule.

RESULTS

There were well-defined Pc 1 events on 20 of the 28 days of the experiment. However, on only 12 of these 20 did the event overlap the 12-hr transmitter operation cycle. Much of the activity during this period can thus be attributed to natural causes.

Before discussing the results which appear to be significant, some comments regarding the Winter Harbor field site are in order. Despite favorable preliminary tests and elaborate precautions, the site proved to have extensive noise problems. The interference was polarized, however, and the difficulties were limited to the vertical and north-south sensors. The east-west sensor appeared to be unaffected. Also this station was dependent on local power, which blacked out on the night of 19 October. Finally, because of the proximity of the Winter Harbor site to the transmitter, the modulated VLF signal was detected by the preamplifiers and is visible as monochromatic signals on the spectral displays. This accident turned out to have fortunate consequences for the visual display of data: during the spectral signal processing, harmonic structure was revealed in the ULF signals.

In Appendix B most of the data from the east-west sensor at Winter Harbor have been spectrally analyzed and displayed on a long time scale. It is useful when viewing the intensified and expanded events which follow to refer to the catalog of data in Appendix B to acquire a sense of perspective with regard to the frequency of occurrence of these micropulsation events.

The events which are the subject of this report subdivide naturally into two classes: possible stimulation and possible enhancement. The first case which may have been an artificially stimulated micropulsation event occurred on 4 October and is illustrated in Fig. 6. This spectral display was constructed from successive photographs of a storage-oscilloscope record of the output of a Federal Scientific spectrum analyzer. The markers at 1.5625 Hz and 3.125 Hz are for frequency calibration, and the spectral line at 0.2 Hz during the periods 0445 - 0500, 0530 - 0600, and 0630 - 0700 (Universal Time is used throughout this report) indicates the transmitter

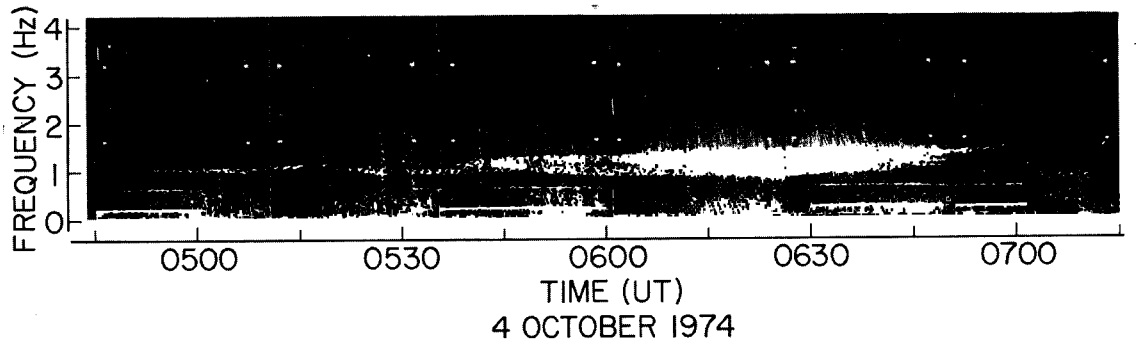

Fig. 6 — Spectral analysis of the Winter Harbor east-west magnetometer signal plotted versus Universal Time for 4 October 1974. The transmitter was modulated at 0.2 Hz from 0430 - 0500, 0530 - 0600 and 0630 - 0700. Note the odd harmonics of the modulation frequency at 0.6 and 1 Hz.

modulation frequency and operating periods. Also visible are the harmonics of the square-wave modulation at 0.6 Hz and 1 Hz. A substantial Pc 1 event ($\approx$ 5 mγ) occurred during this interval, and the display is deliberately saturated in order to trace the beginnings of the event. The latter is seen to have begun in the vicinity of 0500 at nearly the 1-Hz harmonic of the ULF modulation. Indeed, if we expand and intensify the trace (Fig. 7), the micropulsation event first appears superimposed on the faint trace of the 1-Hz harmonic in the time interval 0450 - 0500 and then continues into the period after the transmitter was turned off.

Another micropulsation event which was coincident in time and harmonic frequency with the transmitter occurred on 22 October. On this day a large Pc 1 event was in progress before the transmitter began operation. As shown in Fig. 8a, the event appears to have been dying out until the transmitter was turned on with 0.2-Hz modulation at approximately 0337. There then followed the rapid growth of a micropulsation series at the 0.6-Hz harmonic of the modulation frequency. In Fig. 8b, a marker signal at 0.6 Hz has been inserted to emphasize the close agreement in frequency.

Finally, Fig. 9 illustrates an event on 25 October. Once again the modulation was at 0.2 Hz, and the display has been deliberately saturated to show the initial portions of the event in more detail. This micropulsation series began at 3 Hz, an unusually high frequency for the month's data which were recorded. In fact, there occurred only two events with frequency higher than 2 Hz during the experiment. If we narrow-band filter, expand, and intensify the trace, the result is Fig. 10. In this case the modulation harmonics are visible even as high as 2.6 Hz, and they show that the transmitter came on at 0930. At about 0935 the micropulsation event began at close to 3 Hz. The scarcity of data at these higher frequencies makes it less likely that initiation of the event at a modulation harmonic was a mere chance occurrence.

As an example of what may constitute enhancement effects, Fig. 11 shows an event of 2 October. On this day the modulation frequency was 1 Hz, and an event apparently began in a completely natural fashion at about 1000. As the transmitter came on again at 1030 the micropulsation event appeared to stabilize about the transmitter modulation frequency, and when the transmitter was turned off shortly before 1100, the event disappeared. An expanded picture of the end of the event (Fig. 12) shows that the micropulsation amplitude dropped off rapidly after the transmitter was turned off.

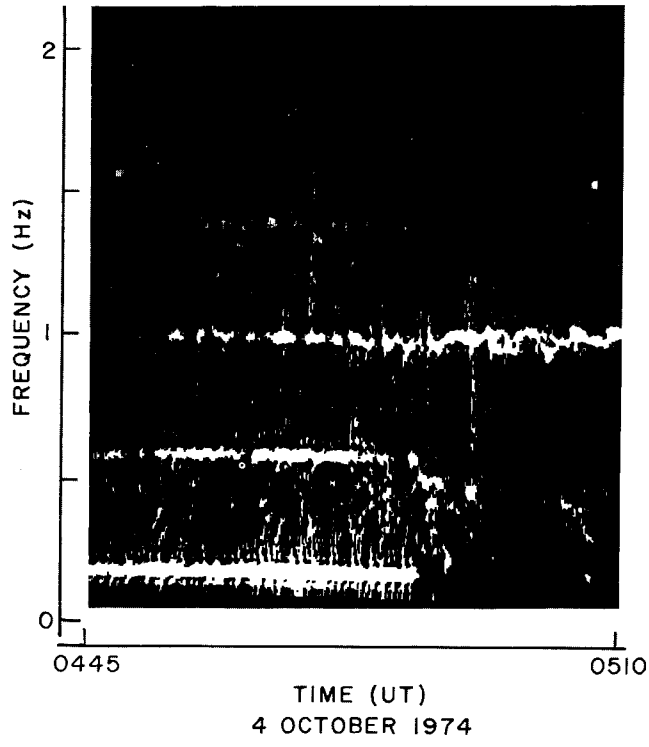

Fig. 7 – Expanded spectral display for the event shown in Fig. 6. The micropulsation event appears to have initiated directly at the 1-Hz harmonic of the transmitter modulation.

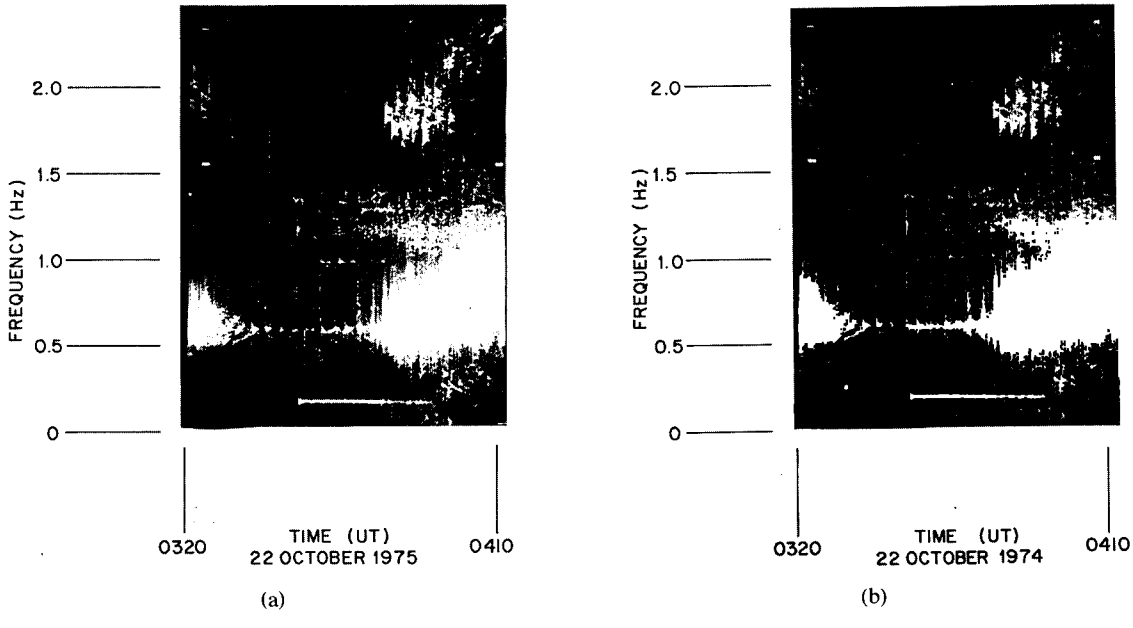

Fig. 8 (a) – Spectral display of the Winter Harbor east-west signal at the beginning of transmitter modulation on 22 October 1974. A micropulsation event in progress appeared to be dying out until the transmitter came on at ~0337 with 0.2-Hz modulation. (b) The addition of a marker frequency at 0.6 Hz shows that the wave growth began directly at the transmitter harmonic.

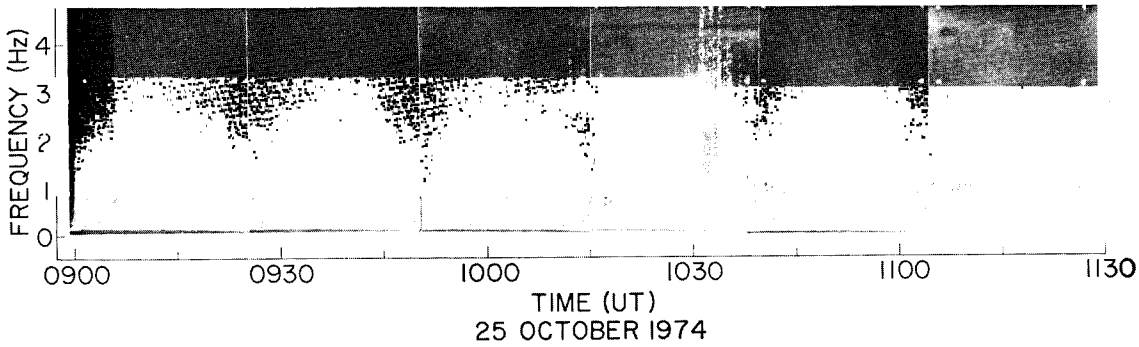

Fig. 9 – Spectral display of Winter Harbor east-west signal for a portion of 25 October 1974. Low-frequency noise obscured the 0.2-Hz transmitter modulation signal which operated 0930 - 1000 and 1030 - 1100. A relatively-high-frequency micropulsation event is shown beginning near 0935.

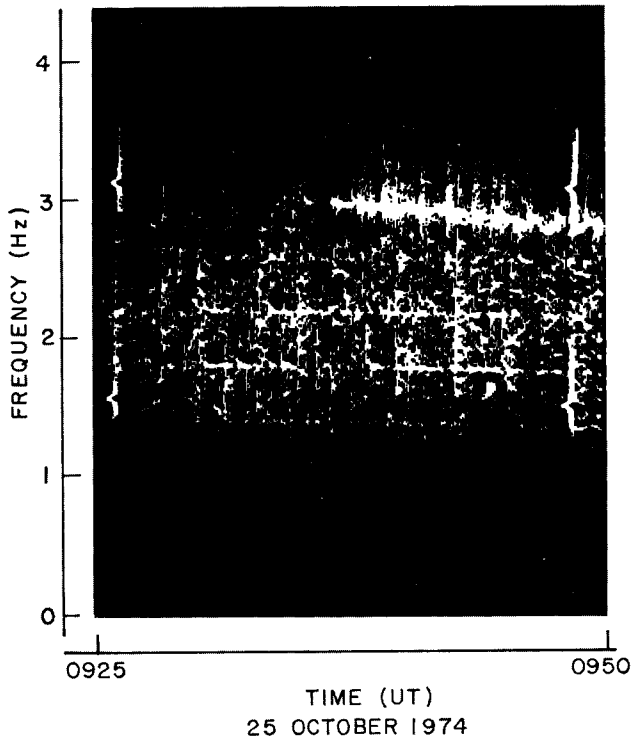

Fig. 10 – Expanded filtered display of the initiation of the micropulsation event in Fig. 4. The modulation harmonics appear at about 0930, followed by the beginning of the micropulsation at about 0935.

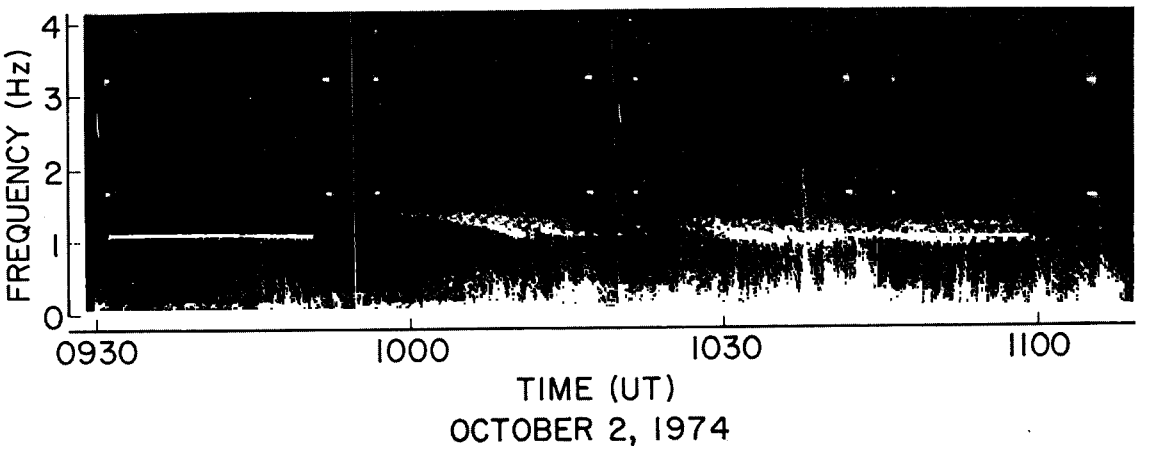

Fig. 11 – Spectral scan of an event from 2 October 1974. The data show transmitter modulation at 1 Hz. The micropulsation event appeared to stabilize at the modulation frequency from 1030 - 1100, ending as the modulation ceased.

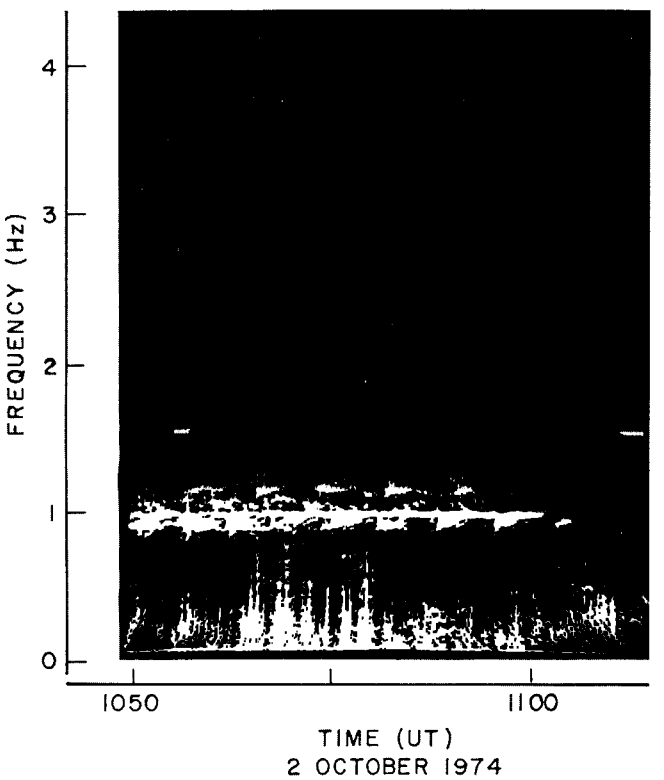

Fig. 12 – Expanded portion of Fig. 6 which shows rapid decrease in event amplitude after the end of modulation

Another case of interest occurred on 4 October with 0.2 Hz modulation. As illustrated in Fig. 13, an event began at about 0940 and ran until after 1100. If we expand the end of this event and look at a skewed, three-dimensional display, better illustrating the amplitude variation (Fig. 14), it is evident that the micropulsation amplitude dropped off monotonically in amplitude after the transmitter was turned off. In this case there is no correspondence in frequency, and the occurrence may indeed be fortuitous.

DISCUSSION

An experiment of this sort bears a resemblance to attempts at rainmaking. In each case, one has difficulty in discriminating between examples of genuine stimulation and events which occurred naturally, and refuge must be sought in statistics. Although the statistics for a month-long study on such relatively infrequent events as Pc 1 micropulsations are necessarily limited, there are some points to be made regarding the possibility that the events discussed previously could have been coincidental.

Micropulsation events frequently extend for an hour or more. If the 12-hr transmitter operating time is divided into 3-hr units, there occurred 112 such units during the experiment. A total of 25 of those units contained micropulsations of detectable magnitude. Broken down into modulation frequencies, events occurred during 10 of 44 operating units at 0.2 Hz, 4 of 32 units at 1 Hz, and 11 of 36 units at 5 Hz. In other words, the four cases at 0.2-Hz modulation which were cited previously as examples of possible stimulation or enhancement represent a significant fraction of the total number of events which occurred when this frequency was being used. On the other hand, no relationship was noted between events which occurred on 5-Hz days and the operation of the transmitter. There were other cases in which stimulation could be argued but which did not show the close agreement in frequency illustrated here. To obtain a true feel for the small number of events from which the data in the previous section were selected, it is probably most useful to view the collected spectral records in Appendix B.

The spectral records in Fig. 6 - 14 have all been taken from the east-west sensor at the Winter Harbor site. Analysis of the data from the other sites showed that the examples of possible

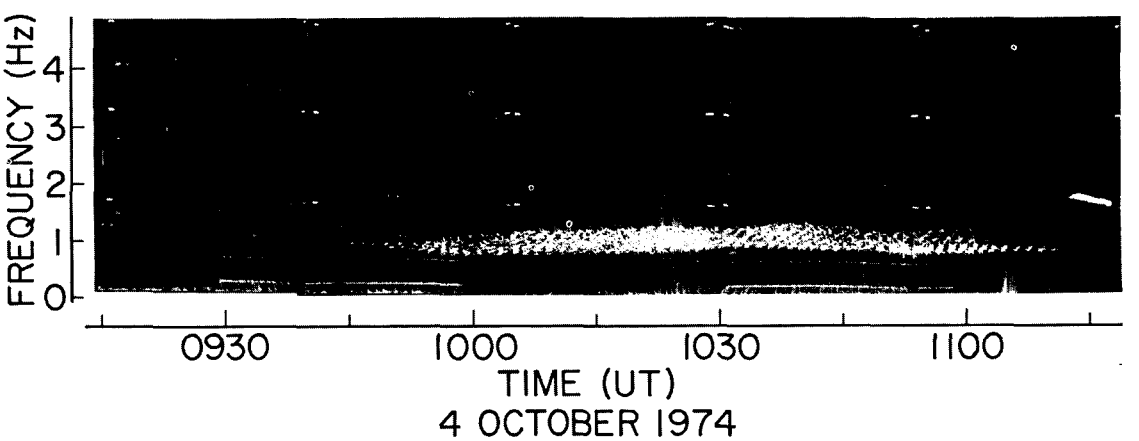

Fig. 13 — Spectral diplay of a micropulsation event from 4 October 1974. Transmitter modulation at 0.2 Hz occurred from 0930 - 1000 and 1030 - 1100. The event monotonically declined in intensity after transmitter shutoff at 1100.

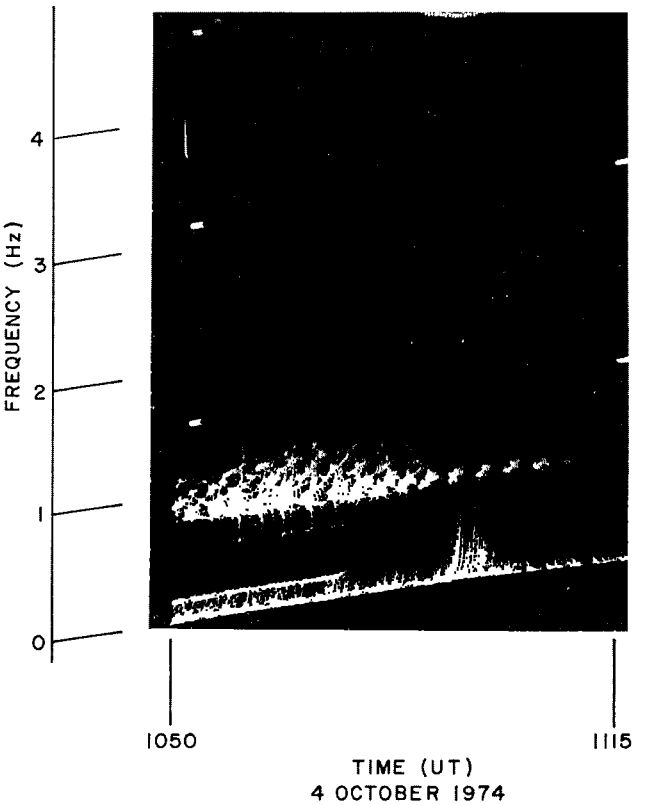

Fig. 14 – Skewed spectral display of a portion of Fig. 8 with amplitude as the third axis shows more clearly the continuous decay in the event amplitude after the transmitter modulation ceases.

stimulation were geographically rather widespread. They were present at all three other sites, with similar start and stop times. The polarization varied widely, however, and in each case the West Virginia station, farthest from the transmitter, recorded the lowest amplitude.

Finally, it is useful to view these events against the general background of geomagnetic activity. Carpenter and Park [21] have proposed an empirical relationship describing the variation of the plasmapause L value (L_{pp}) in terms of the K_p index. They suggested as a crude measure the relationship $L_{pp} = 5.7 - 0.47\overline{K}_p$, where $\overline{K}_p$ is the maximum 3-hr K_p value for the previous 12 hours. This relation ignores diurnal effects, but for the period of transmitter operation (2330-1100 local time), the average variation of the plasmapause position with respect to local time is very small [22]. In Fig. 15, $\overline{K}_p$ is plotted versus time for the entire experiment. The striped regions represent the transmitter operating periods, with the modulation frequency listed at the bottom of the graph. Within the transmitter operating periods, any 3-hr unit which contained a Pc 1 micropulsation is marked with an x. The possible stimulation events are indicated with filled arrows, and the cases of possible enhancement are shown with open arrows. On the right-hand scale, L_{pp} is determined from the empirical formula. The most interesting point raised by this graph is that the possible stimulation events occur in each case on a day of relatively low $\overline{K}_p$ (high L_{pp}) following a day of relatively high $\overline{K}_p$ (low L_{pp}). More specifically, each of the possible

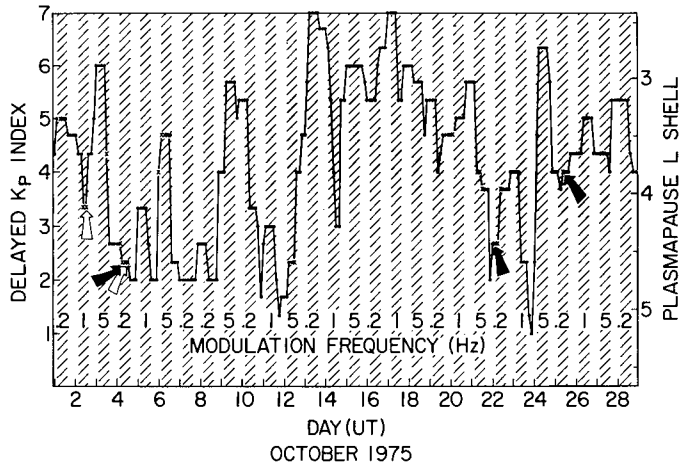

Fig. 15 — A plot of the empirically determined position of the plasmapause (right-hand scale) during the course of the experiment. The transmitter was modulated every other half-hour during the striped intervals at the frequencies shown near the bottom. Three-hour intervals during the transmitter operating periods which contained a micropulsation event are marked with an x. The stimulation events are denoted by black arrows, and the enhancement cases by white arrows.

stimulation cases occurs when the plasmapause L shell has increased to 4 or greater following a depression to 3 or less and the transmitter modulation is at 0.2 Hz; it is worth noting that the relatively-high-frequency event of 25 October does correspond to a lower value of L_{pp}. The actual numbers are probably not significant, but the qualitative behavior may suggest that when the magnetosphere has sufficient energetic protons available, that is, following a disturbance, the likelihood of exciting a micropulsation event is much greater.

The exact mechanism by which large-amplitude, pulse-modulated VLF waves might stimulate ULF waves is open to question. The most reasonable suggestion from these data is that a VLF wave-wave interaction occurs between the carrier and one of the sideband frequencies, yielding a ULF product. The calculation by Harker et al. [19] predicts that the appropriate VLF interaction frequency at these low L values should be closer to 30 kHz rather than the 14.7 kHz used, and additionally that there are serious difficulties with the theory when a realistic plasma temperature is introduced into the model [23]. Further development of this approach is suggested. In any case, it seems likely that the interaction is in the magnetosphere; the effect is not localized to the site nearest the transmitter, as would be expected if it were caused by ionospheric demodulation of the VLF wave.

CONCLUSION

Efforts at stimulating ULF waves by RF heating of the ionosphere under normal conditions were not successful. Our brief experiment in ULF pulse modulation of a high-powered VLF transmitter has yielded several cases of possible stimulation of geomagnetic micropulsation events. The results, though not conclusive, suggest a link between a harmonic of the transmitter modulation and the initiation of a micropulsation event at the frequency of such a harmonic.

This stimulation mechanism appears to be limited to times when the magnetospheric conditions are optimum for the production of Pc 1 micropulsations.

As a consequence of these findings, we conclude that practical means of emitting ULF waves are likely to be limited to conventional means, employing conducting radiators with dimensions of tens to hundreds of kilometers and carrying currents of hundreds to thousands of amperes. In view of the limited information-carrying capacity of ULF waves and in view of their relatively high loss rate in the daytime hemisphere, we believe a practically useful ULF global communications system would be prohibitively expensive by comparison with alternatives in the ELF or higher frequency bands.

ACKNOWLEDGMENTS

The VLF/ULF wave interaction experiments were made possible through the cooperation of the Naval Radio Station at Cutler, Maine. The RF ionospheric heating experiments were conducted with the assistance both of Dr. William Utlaut of the Environmental Science Services Administration Boulder Laboratories and of the Advanced Research Projects Agency. The development of a sensitive and reliable magnetometer system is due primarily to the efforts of William D. Meyers and Edwin L. Althouse of NRL.

APPENDIX A

RADIOFREQUENCY HEATING EFFECTS IN THE LOWER E REGION

We calculate ionospheric perturbations of the type treated in Ref. 14 on the assumption of vertical incidence. This is presumed to be a best possible case; obliquely directed rays will be refracted and tend to reduce the available energy density.

Electron-Temperature Perturbation

The power absorbed per unit volume in the ionosphere is given by

$$Q = Re(\mathbf{J} \cdot \mathbf{E}), \tag{A1}$$

where the current density is specified in terms of the conductivity tensor and the RF electric field:

$$\mathbf{J} = \sigma \cdot \mathbf{E}. \tag{A2}$$

For a particular characteristic mode, ordinary or extraordinary,

$$\mathbf{J}_{\substack{0\\x}} = \sigma_{\substack{0\\x}} E_{\substack{0\\x}} \tag{A3}$$

The $\substack{0\\x}$ subscripts will be suppressed except where they are needed for clarity. From (A1) and (A3) we obtain

$$Q = \frac{1}{2} |E|^2 \, Re(\sigma). \tag{A4}$$

In an inhomogeneous, absorptive medium the electric-field term in the WKB approximation becomes at height z [24]

$$E^2 = \frac{E_0^2}{|n|} \exp - 2k_0 \int_0^z Im(n) \, dz \tag{A5}$$

where n is the effective refractive index of the plasma medium for quasi-longitudinal propagation, k_0 is the free-space wavenumber, and E_0 is the analogous free-space electric field at that height. If we evaluate E_0^2 in terms of the transmitter parameters, the result is

$$E_0^2 = 2\sqrt{\frac{\mu_0}{\epsilon_0} \frac{P_t A_e}{\lambda_0^2 z^2}} \tag{A6}$$

where ϵ_0 and μ_0 are the free-space permittivity and permeability respectively, $P_t A_e$ is the transmitter power-aperture product, and λ_0 is the wavelength in free space.

In a plasma the conductivity can be expressed in terms of an effective refractive index

$$\sigma = i\omega\epsilon_0(1 - n^2). \tag{A7}$$

If we separate the refractive index into real and imaginary parts $n^2 = (\mu + ix)^2$, we obtain

$$Re(\sigma) = 2\omega\epsilon_0(\mu x). \tag{A8}$$

Combining Eqs. (A8), (A6), and (A5) in (A4) we find that the power absorbed per unit volume is given by

$$Q = 2\frac{\omega}{c}\frac{\mu x}{|n|}\frac{P_t A_e}{\lambda_0^2 z^2}\exp - 2k_0\int_0^z x\,dz. \tag{A9}$$

For most of the region of interest, $\mu >> x$ and Eq. (A9) is more simply written as

$$Q = 4\pi x\frac{P_t A_e}{\lambda_0^3 z^2}\exp - 2k_0\int_0^z x\,dz. \tag{A10}$$

For the electron gas of temperature T, conservation of energy yields

$$\frac{dT}{dt} = \frac{Q}{\frac{3}{2}N_e k_B} - (T - T_0)G_m\nu_m, \tag{A11}$$

where G_m is the fraction of excess energy lost per collision, ν_m is the mean electron collision frequency, and the product $G_m\nu_m$ is then just the fraction of excess energy lost per unit time; T_0 represents the ambient unperturbed temperature, k_B is Boltzmann's constant, and N_e is the electron density. In general Q, G_m, and ν_m are not independent of temperature. When nitrogen is the dominant neutral gas, as it is in our case, ν_m and G_m are best represented by [25]

$$\nu_m = \nu_0\frac{T}{T_0} \tag{A12a}$$

and

$$G_m = G_0\left(\frac{T}{T_0}\right)^{-3/2}. \tag{A12b}$$

Q depends on temperature through x, the imaginary portion of the refractive index, which for a wide range of conditions is linearly related to the collision frequency, that is,

$$X = X_0\frac{T}{T_0}. \tag{A13}$$

Thus

$$Q(T) = 4\pi\frac{P_t A_e}{\lambda_0^3 z^2}x_0\frac{T}{T_0}\exp - 2k_0\int_0^z x_0\frac{T}{T_0}\,dz. \tag{A14}$$

Expanding about $T = T_0$ and rewriting the differential equation in terms of $\Delta T = T - T_0$, we obtain

$$\frac{d}{dt}(\Delta T) = \frac{\Delta T_f}{\tau_0}\left[1 - \frac{\Delta T}{T_0}\left(1 - 2k_0\int_0^z x_0\,dz\right)\right], \tag{A15}$$

where only first-order terms are retained, $\tau_0 = (G_0\nu_0)^{-1}$, and $\Delta T_f = Q(T_0)\,2\tau_0/3N_e k_B$.

For times less than the transmitter pulse length, $0 < t < t_{transmitter}$, the solution to Eq.(A15) is given by

$$\Delta T = \frac{\Delta T_f}{R}(1 - e^{-Rt/\tau_0}) = \Delta T_{max}(1 - e^{-t/\tau_1}), \tag{A16}$$

where

$$R = 1 - \frac{\Delta T_f}{T_0}(1 - 2k_0 \int_0^z x_0 \, dz) \tag{A17}$$

and R represents the effect of the explicit temperature dependence in ν and G.

The temperature of the electrons at height z is thus computed to rise to a steady state value of ΔT_{max}, a value which depends on the transmitter power and frequency and on the collision-frequency profile. This change would occur with a time constant τ_1, which is typically on the order of milliseconds. Representative examples will be discussed after treating the related increase in electron density.

Electron Density Perturbations

A rapid change in the temperature of E-region electrons would be expected [13] to lead to an increase in electron density due to a decrease in the rate at which they recombine with the ions. This occurrence can be expressed analytically in terms of the particle-conservation equations. Neglecting diffusion, which is a relatively slow process in the E region, particle density is governed by the following source and loss terms [26]:

$$\frac{dN_e}{dt} = q - \alpha N_e N_m^+ \tag{A18a}$$

$$\frac{dN_m^+}{dt} = \beta N_A^+ - \alpha N_m^+ N_e \tag{A18b}$$

$$\frac{dN_A^+}{dt} = q - \beta N_A^+, \tag{A18c}$$

where N_m^+ and N_A^+ are the molecular and atomic ion densities respectively, q is the rate of production of ionized atoms per unit volume, β is the coefficient for ion-atom interchange, and α is dissociative recombination coefficient. The latter is inversely dependent on temperature [27]. In addition, charge neutrality is guaranteed by

$$N_e = N_A^+ + N_m^+. \tag{A19}$$

If, as suggested by LeLevier [28], a small perturbation ΔT is introduced into Eq. (A18), with the understanding that $\alpha = \alpha_0 T_0/T$, we obtain a differential equation for the resulting density variation:

$$\frac{d}{dt}(\Delta N_e) + 2\alpha N_{e_0} \Delta N_e = \frac{N_{e_0}{}^2 \alpha}{T_0} \Delta T. \tag{A20}$$

If the time dependence calculated in Eq. (A16) is inserted in Eq. (A20), we can solve for the fractional variation in electron density as a function of time after the beginning of the transmitter pulse:

$$\frac{\Delta N_e}{N_{e_0}} = \frac{1\Delta T_{max}}{2T_0}\left[\frac{\tau_2(1 - e^{-t/\tau_2}) - \tau_1(1 - e^{-t/\tau_1})}{\tau_2 - \tau_1}\right]. \tag{A21}$$

To demonstrate the effects of this temperature-density perturbation, we have constructed from a variety of sources [29 - 31] a model ionosphere appropriate to midlatitude, sunspot-minimum conditions. This model is illustrated in Fig. A1 for three different cases. The neutral constituents are presumed to be described by the COSPAR International Reference Atmosphere [32]. Using these representations, the pertinent parameters are listed in Table A1. Note that generally $\tau_1 = R\tau_0$ is much less than τ_2; hence if our attention is confined to longer times such that $\tau_1 << t < \tau_2$, the density perturbation would be expected to vary as

$$\frac{\Delta N_e}{N_{e_0}} \approx \frac{1\Delta T_{max}}{2T_0}(1 - e^{-t/\tau_2}). \tag{A22}$$

In Figs. A2 - A4 the results of these parameters, applied to Eq. (A16), are displayed in terms of the fractional change in electron temperature versus height at three frequencies covering the range of the Platteville transmitter. On the same figures the upper abscissa indicates the corresponding rise times required for the fractional electron-density perturbation to approach one-half the peak fractional temperature change.

From these curves we note that although the predicted temperature variations are much more pronounced in the evening and nighttime cases, the time constant for density variations is correspondingly longer. The effect of the daytime D layer is clearly to severely attenuate the extraordinary and lower frequency modes, leaving the high-frequency waves as most effective for daytime perturbation. As this layer disappears at night, there is an increasing amount of power available in these modes in the E region, until the calculation becomes nonlinear. A nonlinear treatment of heating in the lower ionosphere by Holway and Meltz [33] has confirmed the very large changes in electron temperatures suggested by these linear equations.

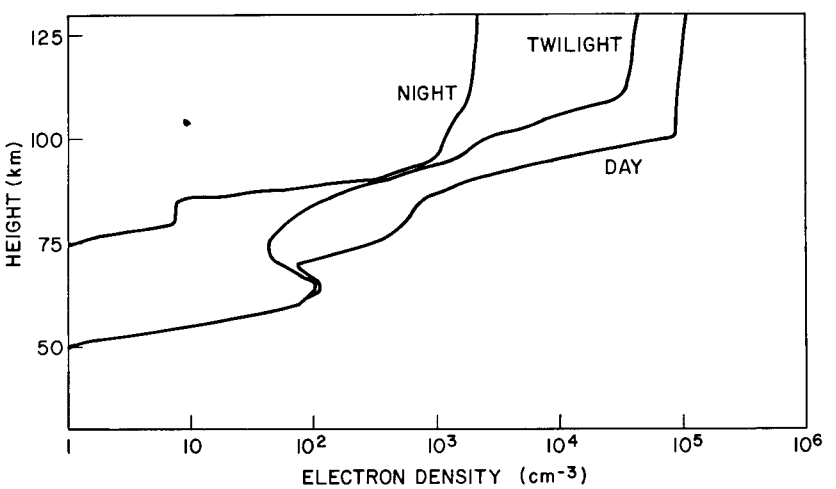

Fig. A1 — Model ionospheric profiles used in the heating calculations

Table A1
Ionospheric-Model Parameters

z (km)	N_e (cm^{-3})		T_0 (K)	ν_M (s^{-1})	α ($cm^3\ s^{-1}$)		τ_0 (ms)	τ_2 (s)		$R(5\ MHz)_o$*	
	Day	Night			Day	Night		Day	Night	Day	Night
60	70	–	243.3	5.5×10^7	–	–	–	–	–	–	–
70	70	1	216.6	1.36×10^7	–	–	–	–	–	–	–
80	590	70	186	2.80×10^6	1.1×10^{-6}	2.4×10^{-5}	–	–	–	–	–
90	2.0×10^3	320	186	4.69×10^5	6.6×10^{-7}	1.2×10^{-6}	0.43	380	1340	0.81	3.5×10^{-3}
100	8.4×10^4	1.2×10^3	213	8.30×10^4	4.3×10^{-7}	7.9×10^{-7}	2.4	14	530	0.98	0.65
110	9.6×10^4	1.8×10^3	263	1.86×10^4	3.1×10^{-7}	5.4×10^{-7}	11	17	520	1	0.79
120	1.0×10^5	2.0×10^3	381	5.48×10^3	2.5×10^{-7}	4.2×10^{-7}	37	20	580	1	0.88
130	1.1×10^5	2.2×10^3	524.3	2.25×10^3	2.0×10^{-7}	3.2×10^{-7}	89	22	707	1	0.93

*Calculation for 5 MHz with ordinary polarization

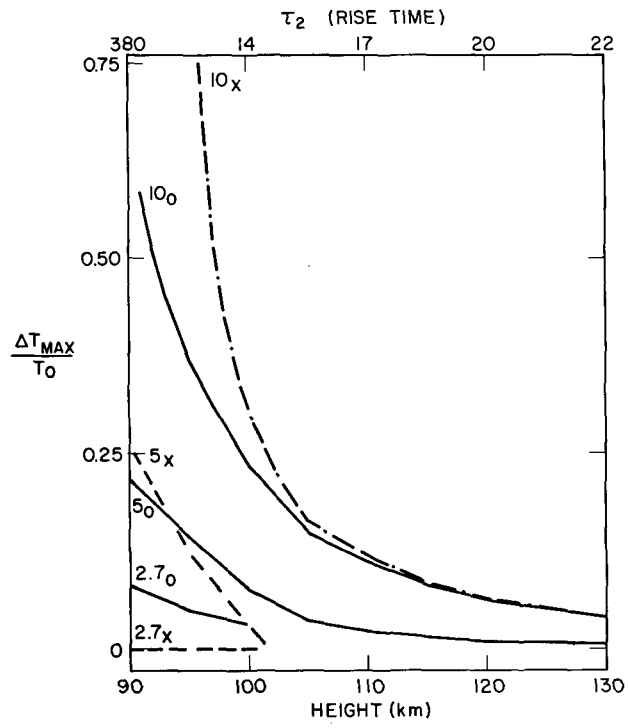

Fig. A2 – Asymptotic values of the fractional variation in electron temperature as a function of height in the daytime E layer for different combinations of frequency and polarization. The time constant for density variation corresponding to each height appears at the top of the graph.

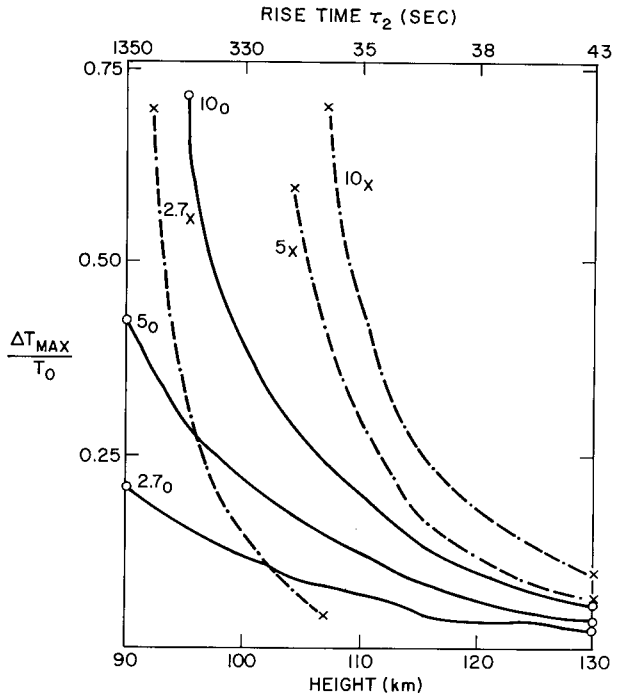

Fig. A3 – Asymptotic values of the fractional variation in electron temperature as a function of height in the twilight E layer for different combinations of frequency and polarization. The time constant for density variation corresponding to each height appears at the top of the graph.

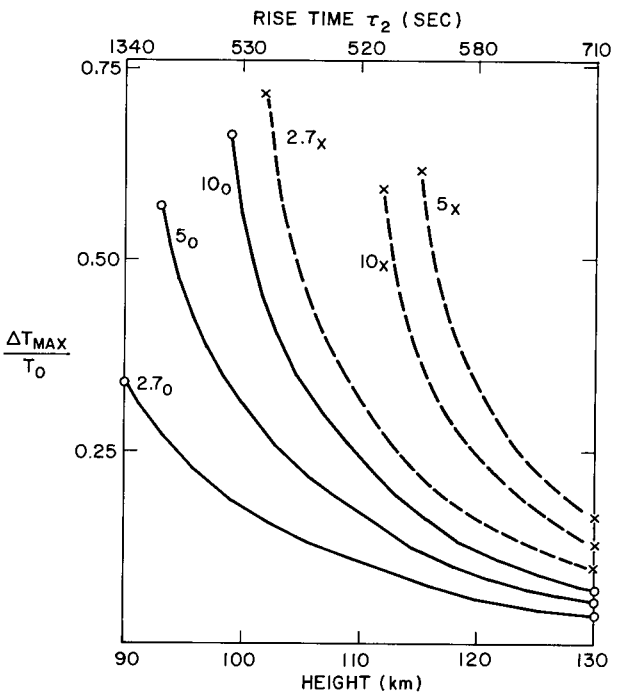

Fig. A4 – Asymptotic values of the fractional variation in electron temperature as a function of height in the nighttime E layer for different combinations of frequency and polarization. The time constant for density variation corresponding to each height appears at the top of the graph.

We are now prepared to return to the original objective, namely, to consider the magnetic perturbations which might be obtainable via the RF heater. The density variations calculated in the preceding are modeled as a cylinder of radius α and density $N_e' = \lambda N_e$ oriented along the background magnetic field $\mathbf{B}_0$ in an otherwise homogeneous ionosphere with density N_e. In this idealized model adapted from Martyn [34], boundary conditions at the cylinder ends are ignored, and the background electric field is presumed to be perpendicular to the cylinder axis. The coordinate system used is illustrated in Fig. A5, where the angle $\sigma = \tan^{-1}(\sigma_2/\sigma_1)$ is determined by the ratio between the Pedersen conductivity σ_1 and the Hall conductivity σ_2. This angle determines the direction of the current density $\mathbf{j}_0$ driven by the ambient electric field $\mathbf{E}_0$. This reference frame is assumed to be at rest with respect to the neutral wind. Within the E region, $\sigma_2 >> \sigma_1$ and α approaches 90°.

The increased conductivity within the overdense cylinder causes a corresponding increase in the current flow through the cylinder. In equilibrium this flow is limited by the polarization electric field which builds up across the cylinder. Invoking continuity of the particle currents and solving the electrostatic boundary-value problem yields a perturbed-current system described by

$$j_x' = \frac{\sigma^2}{\sigma_1} E_0 f(\lambda) \tag{A23a}$$

and

$$j_y' = 0 \tag{A23b}$$

within the cylinder, and outside the cylinder by

$$j_x = \frac{\sigma^2}{\sigma_1} E_0 f(\lambda) \frac{a^2}{\rho^2} \cos 2\varphi \tag{A24a}$$

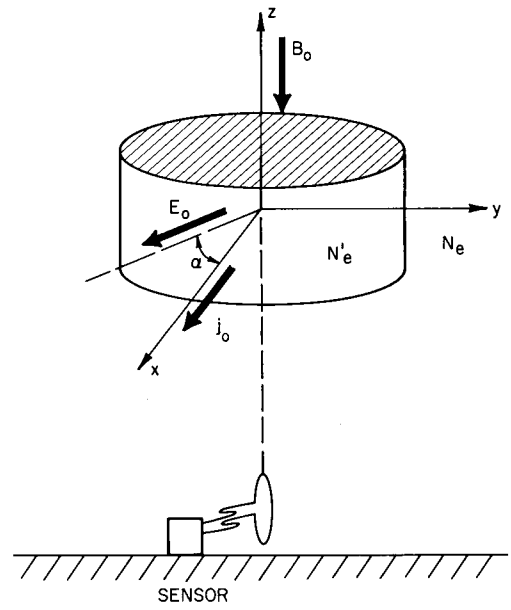

Fig. A5 – Coordinate system used for calculations of the magnetic-field perturbation due to a cyclindrical density irregularity

and

$$j_y = \frac{\sigma^2}{\sigma_1} E_0 f(\lambda) \frac{a^2}{\rho^2} \sin 2\varphi, \tag{A24b}$$

where φ and ρ are the conventional cylindrical coordinates, $\sigma^2 = \sigma_1^2 + \sigma_2^2$, and

$$f(\lambda) = \frac{\lambda - 1}{\left[(\lambda + 1)^2 + (\lambda - 1)^2 \left(\frac{\sigma_2}{\sigma_1}\right)^2\right]^{1/2}}. \tag{A25}$$

This perturbed current system is equivalent to that due to an electric dipole and is sketched in Fig. A6.

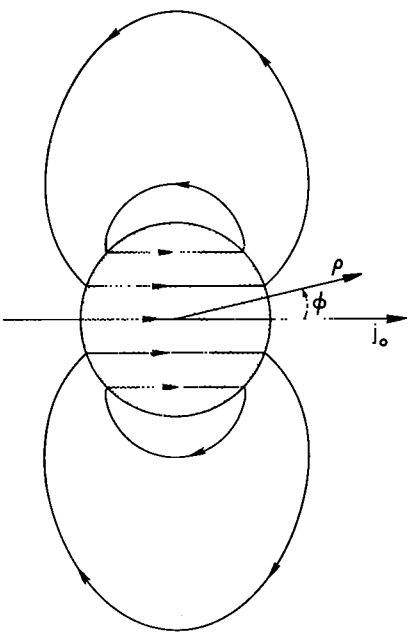

Fig. A6 – The perturbed current system in the horizontal plane

These perturbation currents lead to a variation in the dynamo-generated magnetic fields on the earth's surface. Because the symmetric current terms outside the density enhancement cancel in the volume integration, the magnetic-field disturbance at a point directly below the cylinder at height z is given as

$$\Delta B = \frac{\mu_0}{4\pi} \frac{V_c j_x'}{z^2} E_y$$

where V_c is the volume of the perturbed cylinder. Assuming a background electric field of 10^{-3} V/m and a heated ionospheric region at 100 km height of 30-km diameter and 10-km thickness, we have listed in Table A2 some representative magnetic perturbations which would be anticipated on the basis of the temperature and density calculations presented earlier. Note that the shorter time constant in the daytime seems to more than make up for the smaller temperature variations. Very large nighttime temperature changes for the extraordinary mode could not be

TABLE A2
Estimated Results of Heating as a Function of Time of Day, Polarization, and Transmitter Pulse Length

Model ionosphere	Day		Twilight		Night	
Time constant τ_2 at 100 km (s)	14		331		527	
Frequency and polarization	$(10\ \mathrm{MHz})_0$	$(10\ \mathrm{MHz})_x$	$(10\ \mathrm{MHz})_0$	$(10\ \mathrm{MHz})_x$	$(10\ \mathrm{MHz})_0$	$(10\ \mathrm{MHz})_x$
$\Delta T_{max}/T_0$	22.5%	30.3%	39.7%	NL*	55.3%	NL*
$\Delta N_e/N_e$, 60-s pulse	11%	15%	3.3%	NL*	3.0%	NL*
ΔB(mγ)	7	8	0.1		0.1	
$\Delta N_e/N_e$, 10-s pulse	5.8%	7.8%	0.6%	NL*	0.5%	NL*
ΔB(mγ)	5	6	–		–	
$\Delta N_e/N_e$, 1-s pulse	0.8%	1.1%	0.1%	NL*	0.1%	NL*
ΔB(mγ)	1	1	–		–	

*NL (nonlinear) refers to modes where the perturbed temperature is too large to be treated with the linear theory.

treated by this simple linear model. In any case it appears that distrubances on the order of several milligamma may be generated repetitively by the ionospheric-heating method.

An inherent advantage of this method of controlled modulation of the ionospheric parameters is the possibility of coherent processing to increase the signal-to-noise ratio. Though currently available sensors are capable of detecting signals as low as 1mγ/s, the natural background is also at about this level in the region of 1Hz, and it may well require considerable integration to bring forth a recognizable signal.

APPENDIX B
DATA CATALOG

This appendix is a brief catalog of the micropulsation activity during this experiment, consisting of spectral records for the days on which significant activity was present. Excluded from this record are all the days with 5-Hz modulation (except for Fig. B8, which serves as an example of the lack of activity). Also excluded were days which were too noisy to be of use and the 19 October record (because of a power failure at the Maine site).

These spectral displays were constructed from photographs of the spectra generated by a Federal Scientific signal processor. They are saturated in many places in an attempt to maintain a constant gain at a generally high level. The intent of these figures is to demonstrate that the events which were singled out were not chosen from a large number of occurrences but rather from a small number of events.

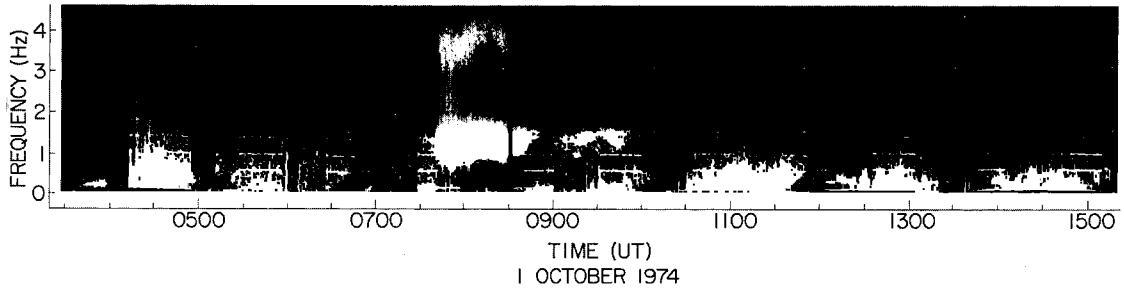

Fig. B1 – Winter Harbor east-west signal, 1 October 1974

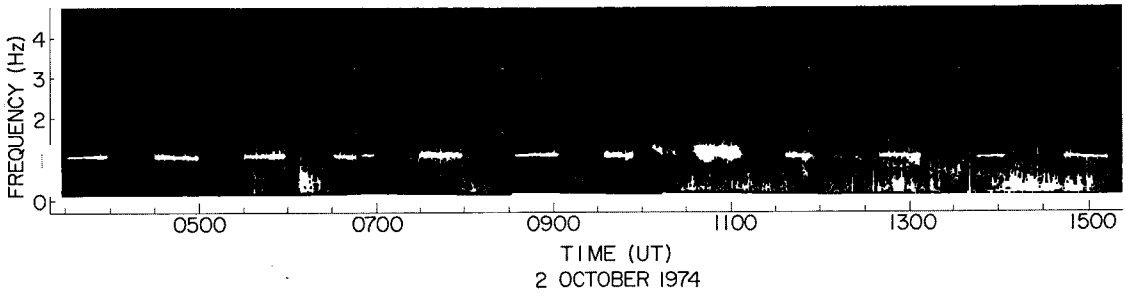

Fig. B2 – Winter Harbor east-west signal, 2 October 1974

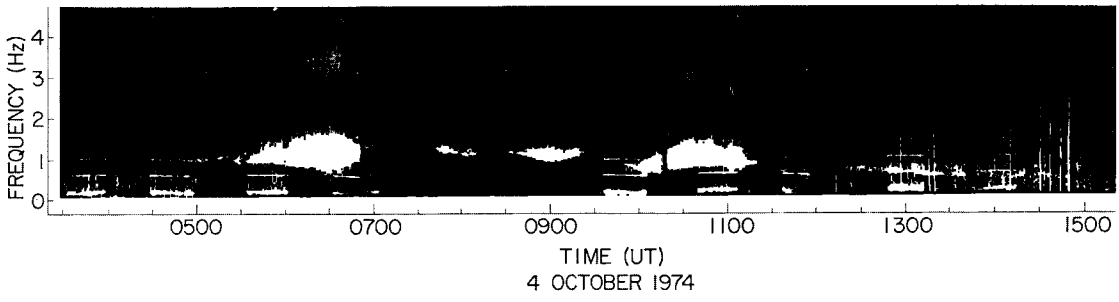

Fig. B3 – Winter Harbor east-west signal, 4 October 1974

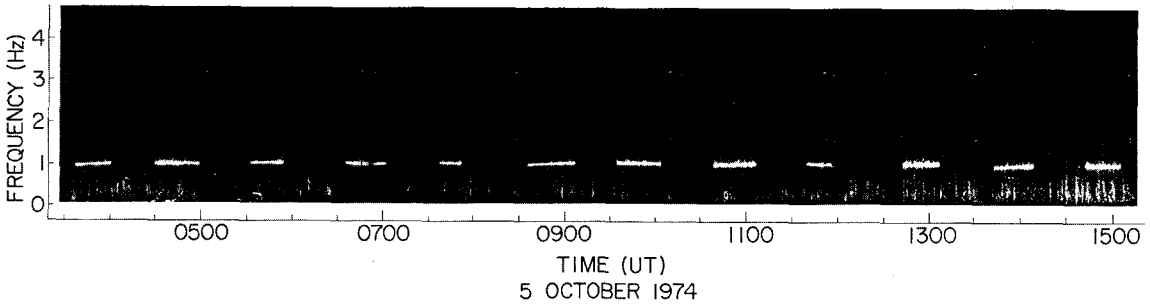

Fig. B4 – Winter Harbor east-west signal, 5 October 1974

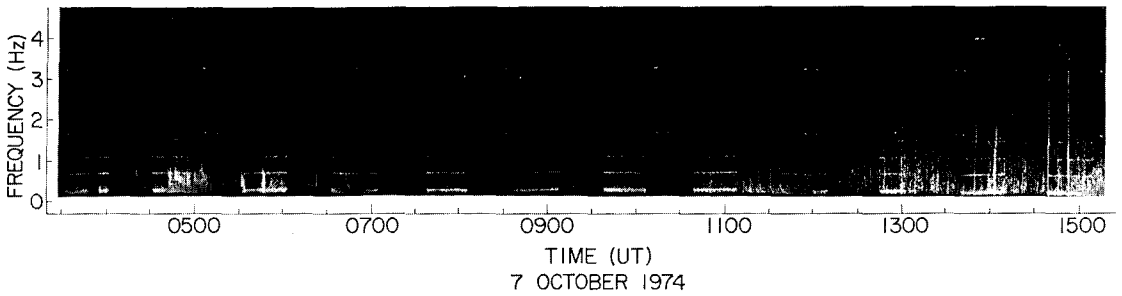

Fig. B5 – Winter Harbor east-west signal, 7 October 1974

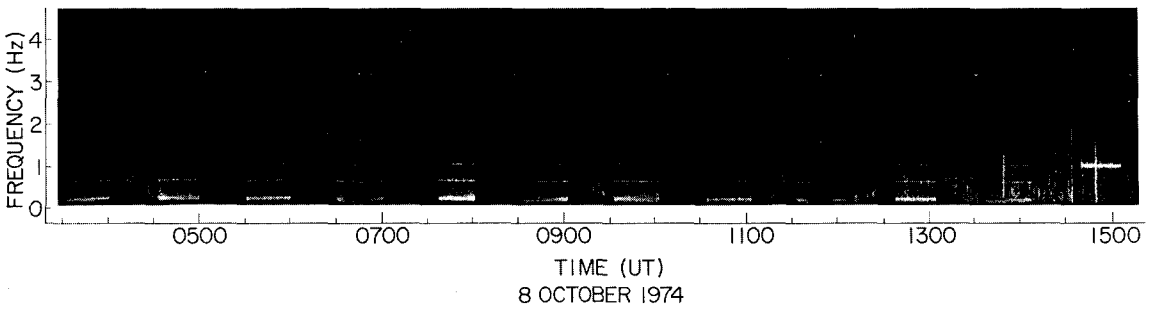

Fig. B6 – Winter Harbor east-west signal, 8 October 1974

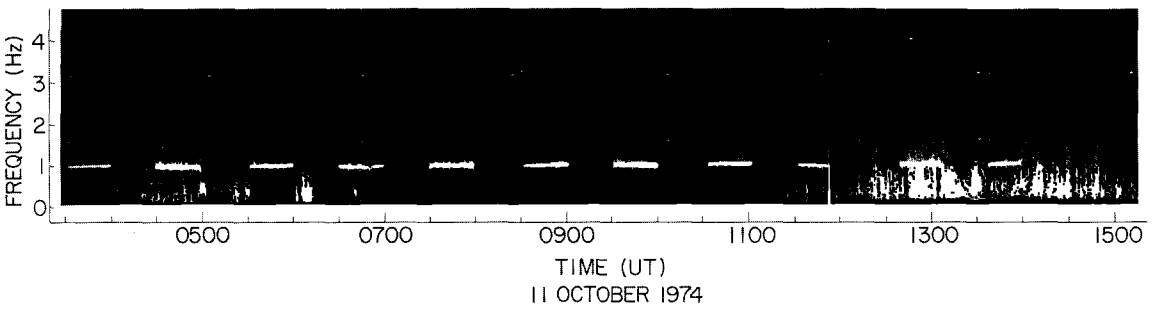

Fig. B7 – Winter Harbor east-west signal, 11 October 1974

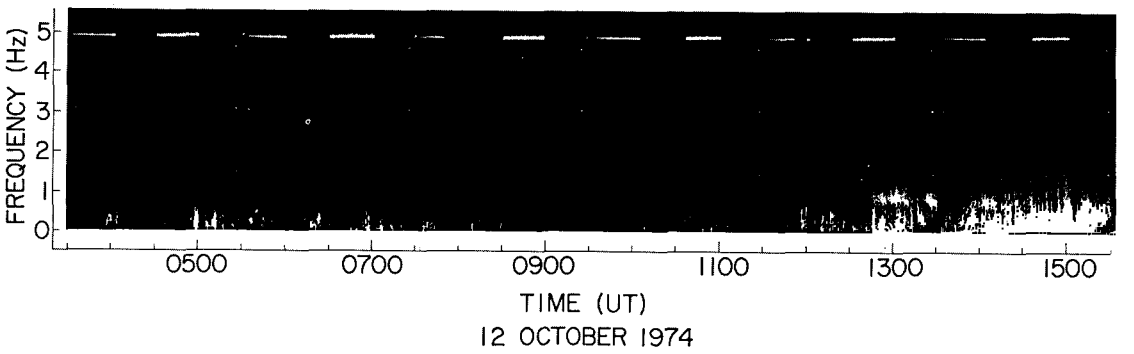

Fig. B8 – Winter Harbor east-west signal, 12 October 1974

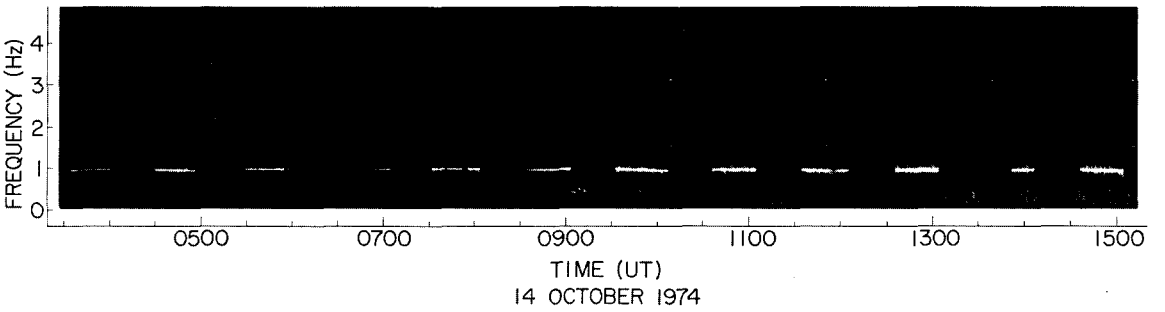

Fig. B9 – Winter Harbor east-west signal, 14 October 1974

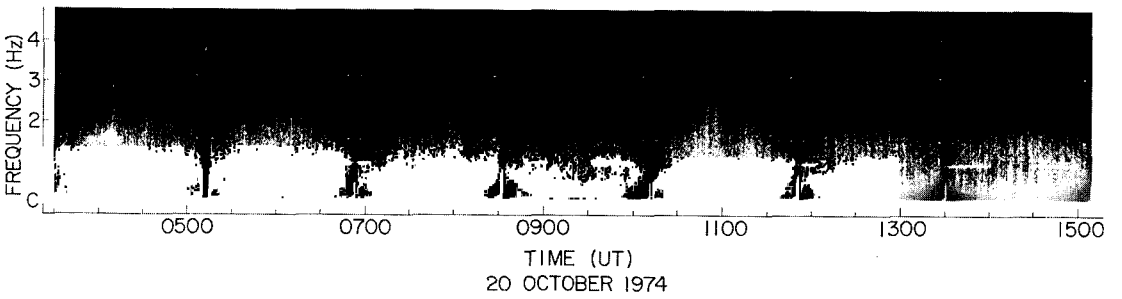

Fig. B10 – Winter Harbor east-west signal, 20 October 1974

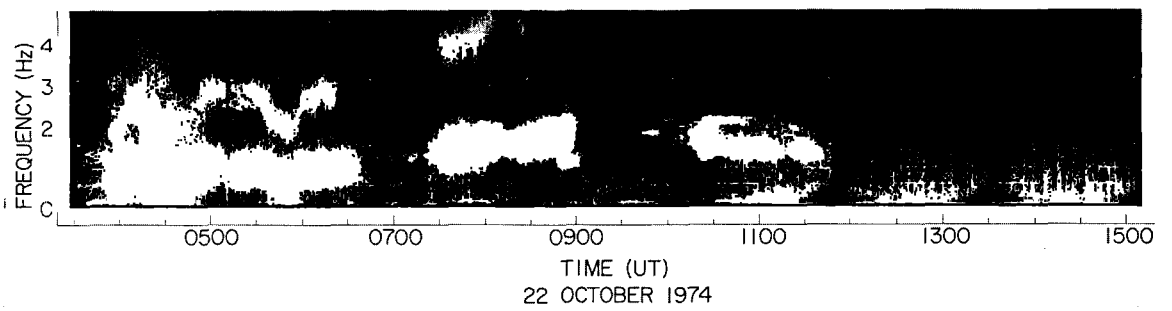

Fig. B11 – Winter Harbor east-west signal, 22 October 1974

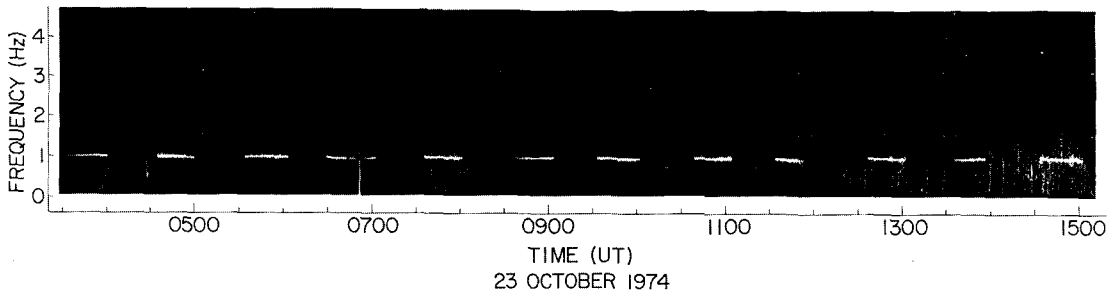

Fig. B12 – Winter Harbor east-west signal, 23 October 1974

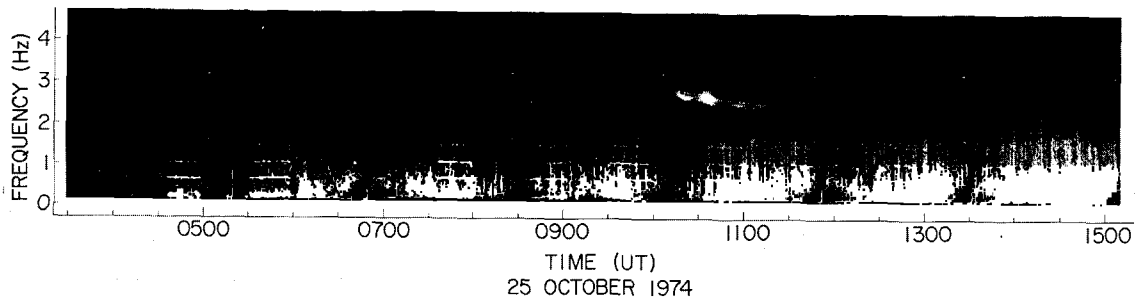

Fig. B13 – Winter Harbor east-west signal, 25 October 1974

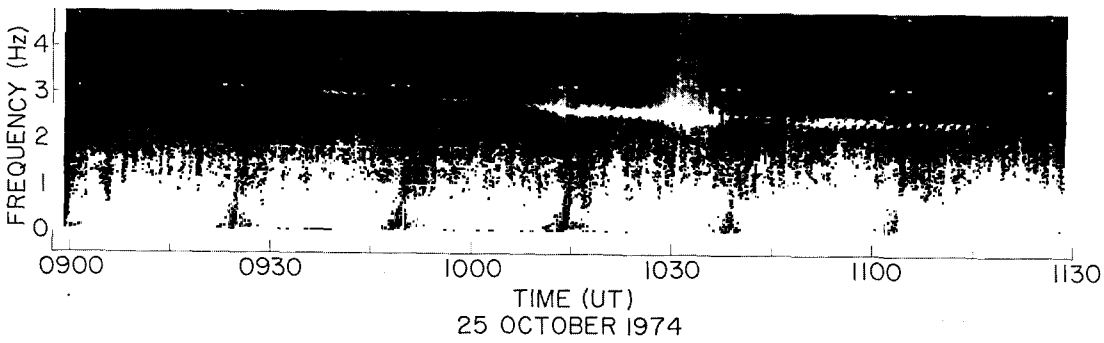

Fig. B14 – Winter Harbor east-west signal, 25 October 1974 (expanded scale)

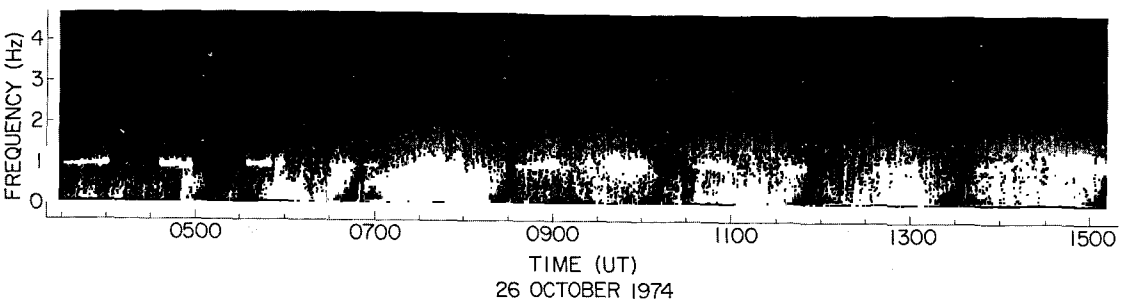

Fig. B15 – Winter Harbor east-west signal, 26 October 1974

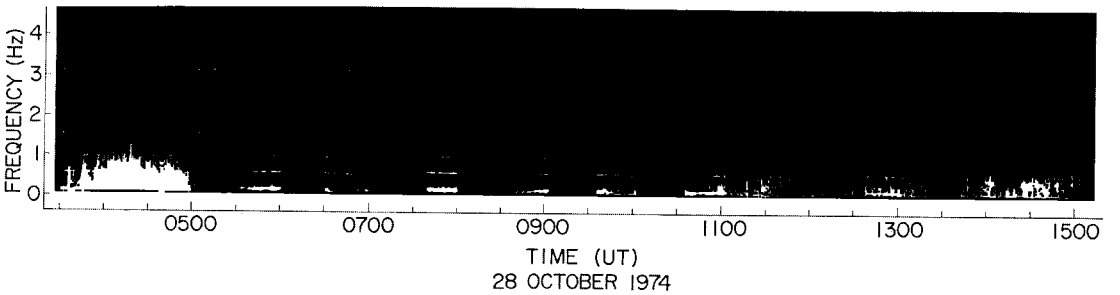

Fig. B16 – Winter Harbor east-west signal, 28 October 1974

REFERENCES

1. J.R. Davis, J.W. Willis, and E.L. Althouse, "Magic Mode: Investigations of Artificial Stimulation of ULF Waves in the Ionosphere and Magnetosphere," NRL Report 7552 (AD759012), Mar. 12, 1973.
2. IEEE Transactions on Communications, Special Issue on Extremely Low Frequency Communications, IEEE Trans. **COM-22,** Apr. 1974.
3. J.A. Jacobs, *Geomagnetic Micropulsations,* Springer-Verlag, New York, 1970
4. H.B. Liemohn, "Cyclotron-Resonance Amplification of VLF and ULF Whistlers," J. Geophys. Res. **72,** 39 (1967).
5. D.R. Criswell, "Pc 1 Micropulsation Activity and Magnetospheric Amplification of 0.2 to 5.0 Hz Hydromagnetic Waves," J. Geophys. Res. **74,** 205 (1969).
6. C. Greifinger and P.S. Greifinger, "Theory of Hydromagnetic Propagation in the Ionospheric Waveguide," J. Geophys. Res. **73,** 7473 (1968).
7. C. Greifinger and P. Greifinger, "Generation of ULF by a Horizontal Electric Dipole," Rad. Sci. **9,** 533 (1974).
8. S. Matsushita and W.H. Campbell, eds., *Physics of Geomagnetic Phenomena,* Academic Press, New York, 1967.
9. W.K. Berthold, A.K. Harris, and H.J. Hope, "World-wide Effects of Hydromagnetic Waves Due to Argus," J. Geophys. Res. **65,** 2233 (1960).
10. C. Greifinger, "Feasibility of Ground-Based Generation of Artificial Micropulsations," J. Geophys. Res. **77,** 6761 (1972).
11. A.C. Fraser-Smith, K.J. Harker, R.T. Bly, and D.M. Bubenik, "Generation of Artificial Geomagnetic Micropulsations with a Large Ground-Based Current Loop," Technical Report SEL-72-023 (AD752061), Stanford Electron. Lab., Stanford, Calif., June 1972.
12. W.F. Utlaut and R. Cohen, "Modifying the Ionosphere with Intense Radio Waves," Science **174,** 245 (1971).

13. A.F. Gurevich, "Disturbance of the Ionosphere by Radio Waves," Geomagn. Aeron. **11** 803 (1971).

14. J.W. Willis and J.R. Davis, "Radio Frequency Heating Effects on Electron Density in the Lower E Region," J. Geophys. Res. **78,** 5710 (1973).

15. T.B. Jones, K. Davies, and B. Wieder, "Observations of D-Region Modifications at Low and Very Low Frequencies," Nature **238,** 33 (1972).

16. A.C. Fraser-Smith and K.R. Roxburgh, "Triggering of Hydromagnetic 'Whistlers' by Sferics," *Planet. Space Sci.,* **17,** 1310-1312, 1969.

17. R. Gendrin, "Substorm Aspects of Magnetic Pulsations," Space Sci. Rev. **11,** 54 (1970).

18. R.A. Helliwell, *Whistlers and Related Ionospheric Phenomena,* Stanford Univ. Press, Stanford, 1965, p. 203.

19. K.J. Harker, F.W. Crawford, and A.C. Fraser-Smith, "Generation of Alfven Waves in the Magnetosphere by Parametric Interaction Between Whistlers," J. Geophys. Res. **79,** 1836 (1974).

20. A.C. Fraser-Smith and C.A. Cole, Jr., "Initial Observations of the Artificial Stimulation of ULF Pulsations by Pulsed VLF Transmissions," Geophys. Res. Lett. **2,** 146 (1975).

21. D.L. Carpenter and C.G. Park, "On What Ionospheric Workers Should Know About the Plasmapause-Plasmasphere," Rev. Geophys. Space Phys. **11,** 133 (1973).

22. H.A. Taylor, Jr., H.C. Brinton, and A.R. Deshmukh, "Observations of Irregular Structure in Thermal Ion Distributions in the Duskside Magnetosphere," J. Geophys. Res. **75,** 2481 (1970).

23. J.W. Willis, "Temperature Effects on Whistler Modes Near Gyroresonance," J. Geophys. Res. **80,** p. 1354 (Apr. 1975).

24. K.G. Budden, *Radio Waves in the Ionosphere,* Cambridge University Press, Cambridge, 1961.

25. M.H. Mentzoni and R.V. Row, "Rotational Excitation and Electron Relaxation in Nitrogen," Phys. Rev. **130,** 2312 (1963).

26. H. Rishbeth and O.K. Garriott, *Introduction to Ionospheric Physics,* Academic, New York, 1969, p. 113.

27. A.P. Mitra and P. Banerjee, "Models for the Effective Recombination Coefficients in the Ionosphere," Space Res. **9,** 1019 (1971).

28. R.E. LeLevier, "Artificial Heating of the Ionosphere—Early Time Phenomena," J. Geophys. Res. **75,** 6419 (1970).

29. W.B. Hanson, "Structure of the Ionosphere," in *Satellite Environment Handbook,* F.S. Johnson, editor, Stanford Univ. Press, Stanford, 1965, p. 21.

30. D.G. Deeks, "D-region Electron Distributions in Middle Latitudes Deduced from the Reflexion of Long Radio Waves," Proc. Roy. Soc. (London) **A291,** 413 (1966).

32. *COSPAR International Reference Atmosphere,* North-Holland, Amsterdam, 1965.

31. W.E. Sims and F.X. Bostick, "Atmospheric Parameters for Four Quiescent Earth Conditions," Elec. Eng. Res. Lab., Univ. of Texas, Austin, Report; 132, Sept. 1, 1963.

33. L.H. Holway, Jr., and G. Meltz, "Heating of the Lower Ionosphere by Powerful Radio Waves," J. Geophys. Res. **78,** 8402 (1973).

34. D.F. Martyn, "Electric Currents in the Ionosphere, Part III: Ionization Drift Due to Winds and Electric Fields," Phil. Trans. Roy. Soc. (London) **A246,** 306 (1953).